ELSEVIER

Research paper

# Combining BNCT with carbonic anhydrase inhibition for mesothelioma treatment: Synthesis, *in vitro, in vivo* studies of ureidosulfamido carboranes

Alberto Lanfranco [a,1], Sahar Rakhshan [b,1], Diego Alberti [b], Polyssena Renzi [a], Ayda Zarechian [b], Nicoletta Protti [c,d], Saverio Altieri [c,d], Simonetta Geninatti Crich [b,**], Annamaria Deagostino [a,*]

[a] *Department of Chemistry, University of Torino, Via P. Giuria, 7, 10125, Turin, Italy*
[b] *Department of Molecular Biotechnology and Health Sciences, University of Torino, Via Nizza, 52, 10126, Turin, Italy*
[c] *Department of Physics, University of Pavia, Via Agostino Bassi 6, 27100, Pavia, Italy*
[d] *Nuclear Physics National Institute (INFN), Unit of Pavia, Via Agostino Bassi 6, 27100, Pavia, Italy*

A R T I C L E   I N F O

A B S T R A C T

Mesothelioma is a malignant neoplasm of mesothelial cells caused by exposure to asbestos. The average survival time after diagnosis is usually nine/twelve months. A multi-therapeutic approach is therefore required to treat and prevent recurrence. Boronated derivatives containing a carborane cage, a sulfamido group and an ureido functionality (CA-USF) have been designed, synthesised and tested, in order to couple Boron Neutron Capture Therapy (BNCT) and the inhibition of Carbonic Anhydrases (CAs), which are overexpressed in many tumours. *In vitro* studies showed greater inhibition than the reference drug acetazolamide (AZ). To increase solubility in aqueous media, CA-USFs were used as inclusion complexes of hydroxypropyl β-cyclodextrin (HP-β-CD) in all the inhibition and cell experiments. BNCT experiments carried out on AB22 (murine mesothelioma) cell lines showed a marked inhibition of cell proliferation by CA-USFs, and in one case a complete inhibition of proliferation twenty days after neutron irradiation. Finally, *in vivo* neutron irradiation experiments on a mouse model of mesothelioma demonstrated the efficiency of combining CA IX inhibition and BNCT treatment. Indeed, a greater reduction in tumour mass was observed in treated mice compared to untreated mice, with a significant higher effect when combined with BNCT. For *in vivo* experiments CA-USFs were administered as inclusion complexes of higher molecular weight β-CD polymers thus increasing the selective extravasation into tumour tissue and reducing clearance. In this way, boron uptake was maximised and CA-USFs demonstrated to be *in vivo* well tolerated at a therapeutic dose. The therapeutic strategy herein described could be expanded to other cancers with increased CA IX activity, such as melanoma, glioma, and breast cancer.

## 1. Introduction

Malignant pleural mesothelioma (MPM) is an aggressive malignancy with no effective cure. It presents a poor diagnosis, and it is associated with respiratory symptoms and a history of asbestos exposure [1]. The treatment of MPM is evolving, and a multidisciplinary approach of surgical resection, chemotherapy, and radiation therapy it is considered the optimal strategy [2]. Cancer treatments with a single therapeutic agent often result in limited clinical outcomes due to tumour heterogeneity and drug resistance [3,4], especially for more aggressive and metastasising cancer cells [5]. Drug inactivation, apoptosis evasion,

enhanced deoxyribonucleic acid (DNA) repair, increased drug efflux and epithelial-to-mesenchymal transition are the main mechanisms involved in chemoresistance. Among them, the tumour microenvironment (TM) is now considered a critical point in cancer initiation and progression [6, 7]. Thus, the choice of a multimodal therapeutic approach can additively increase anti-cancer activity, concurrently lower the doses of each agent, hence, reducing side effects [8]. The ability of some substances to inhibit enzymes, which are essential for cancer cells growth, can be exploited in targeted therapies. Carbonic Anhydrases (CAs) are wide-spread zinc enzymes playing a central role in both transport and metabolic processes [9]. Sixteen different α-CA isoenzymes and related

proteins (CARP) have been found in mammals with different subcellular localization and tissue distribution. Moreover, for solid tumours, it has been demonstrated that CAs have a fundamental role in maintaining the acidity of the tumour environment by exploiting both $CO_2$ and bicarbonate. Thus, CAs are under special attention, considering that low extracellular pH is associated with tumour progression and chemoresistance by decreasing the uptake of weakly-basic anticancer drugs [10–12].

Recently, two CA isozymes have been prominently associated with cancer: CA IX and CA XII [13–15]. The first, CA IX, is scarcely present in normal tissues and is overexpressed in a large variety of cancer cells. In contrast, CA XII, which is more abundant in normal tissues, has recently been shown to be co-expressed with CA IX in several tumour tissues. The CA XII expression is also induced by hypoxia, but the underlying molecular mechanism still remains unknown. CAs are primarily inhibited by two main classes of compounds: metals complexing inorganic anions (*e.g.* cyanide, cyanate, thiocyanate, azide, hydrogensulphide) and the unsubstituted sulfonamides ($RSO_2NH_2$) [16,17]. As shown in Fig. 1 left, many sulfonamide-based drugs are clinically used in the treatment of different pathological conditions. In particular, aromatic sulfonamides have been shown to reverse the effect of tumour acidification and to inhibit the growth of cancer cells with 50% Grown Inhibition ($GI_{50}$) values in the micromolar range [18].

Unfortunately, all the classical CA inhibitors do not selectively target CA IX and XII because of their ability to inhibit other CA isozymes (*i.e.* CA I and II) having a physiological relevance. To overcome this problem, it is necessary either to elaborate new strategies or to design new structures where the sulfamido group is coupled to another functionality able to direct the drug activity toward an effective and selective inhibition of CAs IX/XII.

Recently, ureido-substituted benzenesulfanilamides have demonstrated excellent inhibitory effects for several human CAs (hCAs) such as the cytosolic isoforms I and II and hCAs IX and XII (transmembrane, tumour-associated enzymes) due to the presence of an urea moiety [19–22]. Interestingly, a derivative including the ureido functionality, and inspired to the drug Sorafenib© showed a selective inhibition of hCA IX, with inhibition constant ($K_I$) values in the low nanomolar ranges [23–25]. On these bases, new ureidosulfamido-based structures have been recently proposed as CAs inhibitors (Fig. 1 right, compounds I-III) [26,27]. Among these derivatives, compound II (SLC-0001 in Fig. 1) bearing a fluorine atom in the *para*-position of the phenyl substituted ureido moiety, showed a good selectivity towards CA IX. Thanks to its *in*

*vivo* antimetastatic effect on breast cancer, it is currently under phase II clinical trials. Interestingly, previous studies pointed out also the *meta*-nitrophenyl ureidobenzenesulfonamide III as one of the most promising inhibitors with a $K_I$ for CA IX of 0.9 nM and a high CA II/CA IX selectivity [28]. Furthermore, to complement the treatment and/or intensify drug toxicity, the use of CA IX inhibitors is often proposed in combination with other chemo- or radio-therapies [29].

Among innovative therapeutic strategies, Boron Neutron Capture Therapy (BNCT) is an experimental radiotherapy which combines low energy thermal neutron irradiation with the presence of boron 10 ($^{10}$B) enriched agents accumulated in the targeted pathological tissues. Upon the neutron capture event, $^{10}$B is converted into non-stable $^{11}$B nuclei [30–33], which disintegrate into α-particles and 7Li. Thanks to the short ionisation ranges (5–9 μm), the charged particles cause irreversible damages specifically to the cell where they were produced, while sparing the surrounding healthy tissues. This property makes BNCT an example of a promising targeted therapy, exhibiting good efficacy and low toxicity, providing tumour-selective cell death. BNCT has been proposed for the treatment of mesothelioma, by the use of a BSH-hyaluronan formulation [33,34]. Among boron derivatives for BNCT, carboranes, icosahedral clusters containing boron, carbon, and hydrogen, occupy a special position both for their high boron content and their chemical versatility coupled with a high *in vivo* stability [35, 36]. Moreover, they are considered bulky pharmacophores which can replace various hydrophobic structures in biologically active molecules [37]. Carboranes, in fact, enhance hydrophobic interactions with receptors conferring stability towards catabolism and degradation by enzymes [38–40].

For this reason, over the years, the use of boron clusters as components of new pharmacological agents has been increasing [41–46]. In 2013, for the first time, and later in 2020 [47,48], Grüner et al. reported high selective carborane-based CA IX inhibitors showing subnanomolar inhibition constant. More recently, the same research group reported similar results with cobalt bis(dicarbollide) alkylsulfonamides [49,50]. Furthermore, the nature of the interactions between CA II and carborane-sulfonamide inhibitors has been investigated [51–54]. Inspired by these studies, and exploiting our experience on MRI-BNCT theranostics as antitumoral agents [55,56], in 2020, we presented $^{10}$B-enriched sulfamido carborane **CA SF** (CA-SF, Fig. 1), as a potential multivalent anticancer agent with the scope of additively couple the inhibition effect of CA with the application of BNCT. **CA-SF** effectively hampered the growth of mesothelioma and breast cancer cells, its
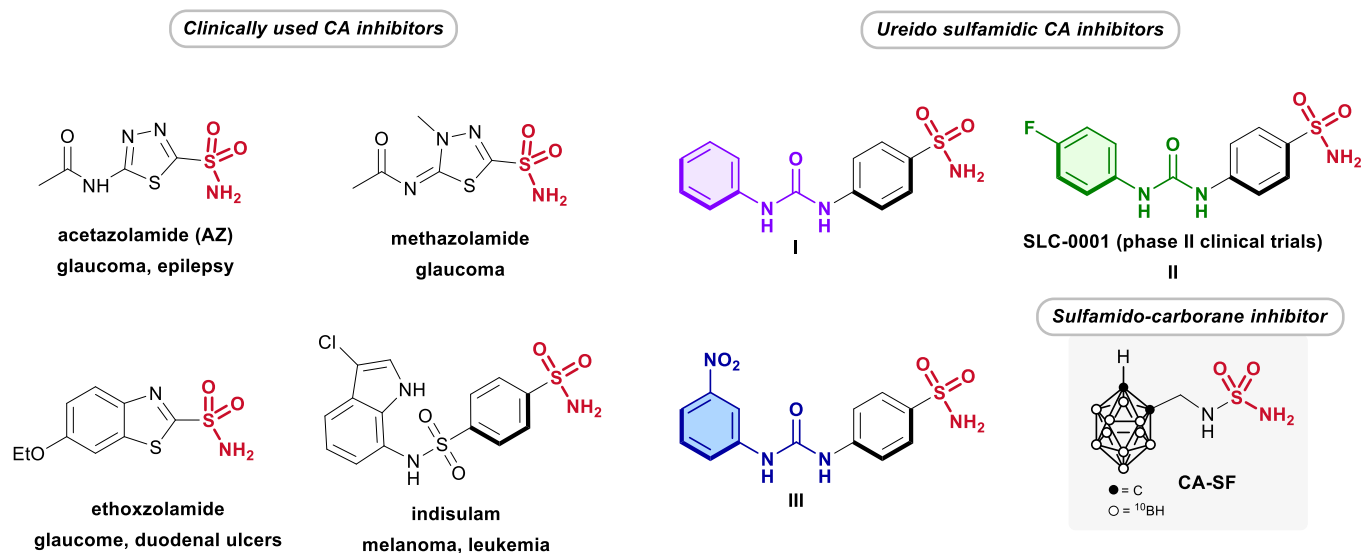


**Fig. 1.** Summary of clinically used CA inhibitors (left), ureido sulfamidic CA inhibitors **I-III** and sulfamido carborane **CA-SF** (right) previously reported.

cellular uptake showed an additive toxic effect upon the application of BNCT that, in the case of mesothelioma, was not able to completely stop cell growth. Most important, the *in vivo* experiments showed a limited mesothelioma tumour re-growth in the case of CA-SF treated and irradiated mice [57].

In this study, we propose the rational design, synthesis and application of new dual agents, namely substituted ureidosulfamido-carboranes (**CA-USFs**), with the aim to selectively target mesothelioma cancer cells overexpressing CA IX and reducing or eliminating their re-growth exploiting the additive effect of a targeted radiotherapy such as BNCT. As shown in Scheme 1, this target can be obtained by derivatising the sulfamido-carborane **CA-SF** on the second carbon atom, with an ureido moiety substituted with a phenyl ring bearing a fluorine or a nitro group, as previously shown for the ureido sulfamidic CA inhibitors **I-III**. The unsubstituted compound **CA-USF** is employed as a reference for the evaluation of the CA inhibitory activity. A combined therapy is fundamental to fight against chemo- and radio-resistance of mesothelioma tumour cells, since the available therapies to counter mesothelioma can only guarantee a survival expectation of less than one year [1].

## 2. Results and discussion

### 2.1. Synthetic strategy to obtain substituted CA-USFs

In order to install the ureido and the sulfamidic groups on the carborane cage, the orthogonally protected diamino carborane **7**, a versatile platform previously reported by our research group for the preparation of several antitumoral and theranostic agents, was exploited [54]. As shown in Scheme 2, diamino carborane **7** is obtained by two key Mitsunobu reactions, allowing the straightforward introduction of the suitable protected amino groups from alcohol **1**. The orthogonally protected alkyne **6** was then exploited to introduce the carborane cage *via* dehydrogenative insertion on decaborane.
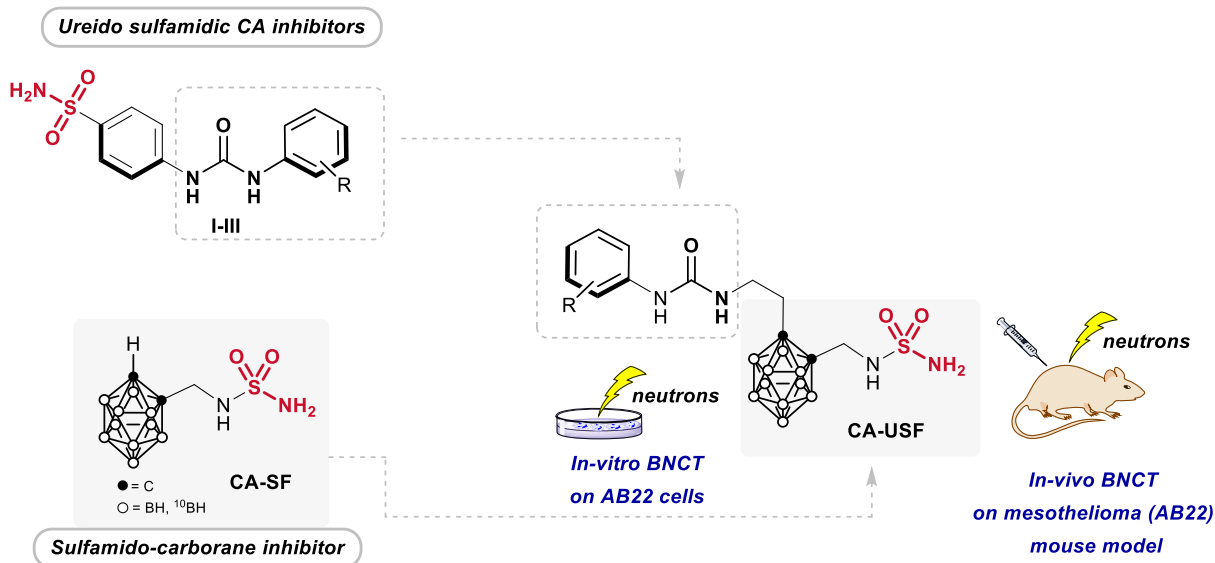
Once intermediate **7** was obtained, carboxybenzyl protection was removed by catalytic hydrogenation in acidic environment to avoid the degradation of the cage, being the free amine strongly nucleophilic.

Indeed, *ortho*-carboranyl hydrochloric salt **8** was obtained in nearly quantitative yields by a simple filtration. Derivative **8** was used for the following reaction, with the suitable arylisocyanate without further purification.

Arylureidosulfamido *ortho*-carboranes were obtained in very good yields, ranging from 90% in the case of **9a** to 87% for **9b** and 85% for **9c**. At this point, phthaloyl group was removed by reduction with NaBH$_4$, followed by acidic treatment affording derivatives **10a-c** in excellent yields (**10a** 90%, **10b** 99%, **10c** 85%). $^1$H and $^{13}$C NMR spectra confirmed the success of the reaction, by the disappearance of the aromatic signals. The last step of the synthetic sequence concerned the introduction of the sulfamido group by the reaction of intermediate **10** with sulfamide in 1,4-dioxane at reflux. **CA-USFs** were successfully obtained in yields (**CA-USF** 48%, **F-CA-USF** 55%, **NO$_2$-CA-USF** 56%) which are consistent with the yields obtained for similar *ortho*-carborane derivatives [57]. Probably, the moderate obtained yields are due to the instability of the carborane cage in the presence of nucleophilic groups and to the relatively harsh conditions necessary for the introduction of the sulfamido group, occurring through the release of a quite poor leaving group. The shift of the methylene signals adjacent to the amino group in **10a-c** and to the sulfamido group in **CA-USFs** in $^1$H and $^{13}$C NMR spectra witnessed the formation of the desired ureidosulfamido-*ortho*-carboranes. In order to perform a BNCT treatment, $^{10}$B-enriched **CA-USFs** have been synthesised. Intermediate **6**, bearing two orthogonally protected amino groups, was subjected to the dehydrogenative insertion using $^{10}$B-enriched decaborane, affording carborane $^{10}$**B-7** in 53% yield. The catalytic hydrogenation allowed the isolation of the hydrochloric salt $^{10}$**B-8** in almost quantitative yield. This latter was reacted with the suitable isocyanate in yields comparable to the non-enriched compounds. Once $^{10}$**B-9b-c** were obtained, the phthaloyl group removal and the reaction with sulfamide afforded $^{10}$**B-F-CA-USF** and $^{10}$**B-NO$_2$-CA-USF** in 56 and 58% yields, respectively. Since **CA-USF** did not show promising *in vitro* results and it was mainly used as a reference, its $^{10}$B-enriched analogue was not synthesised.



**Scheme 1.** This work: rational design of ureidosulfamido-carborane (**CA-USFs**) inhibitors and their *in vitro* and *in vivo* application for mesothelioma treatment.
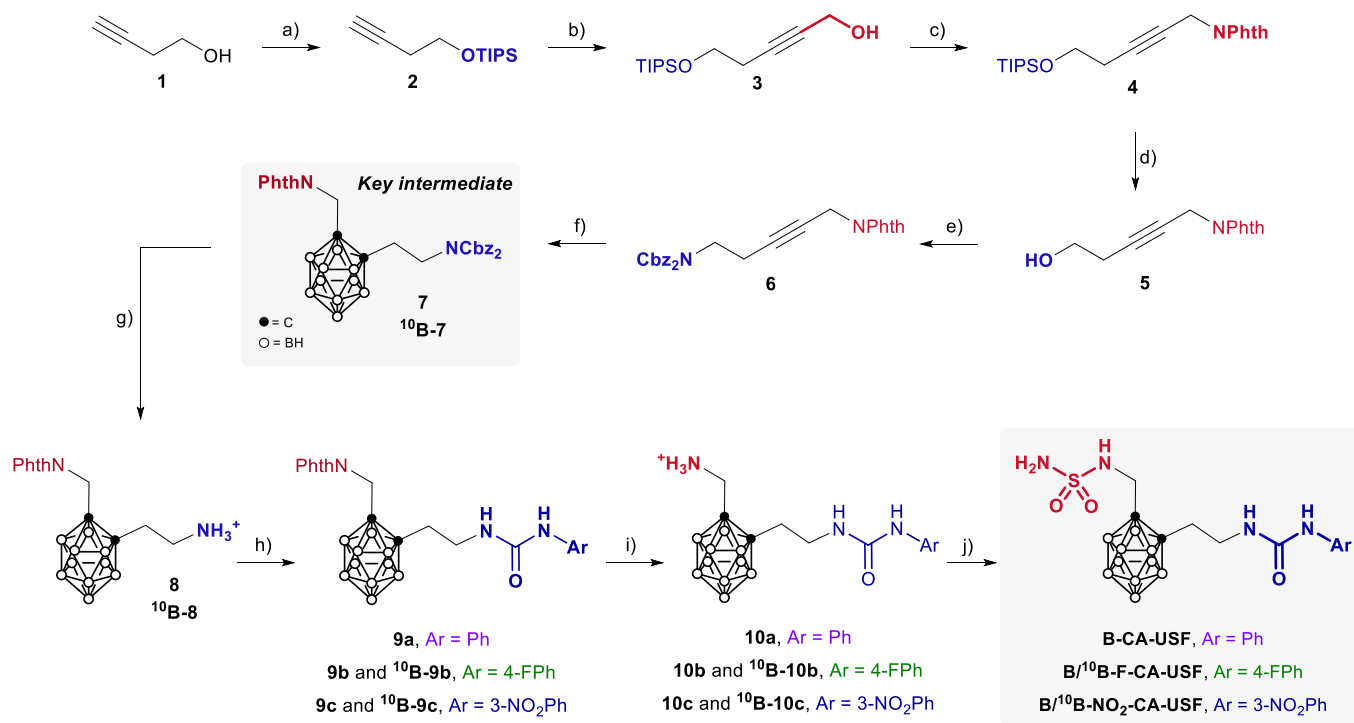
**Scheme 2.** Synthesis of **CA-USFs**. Reaction conditions and yields: a) TIPSCl, imidazole, anhydr. $CH_2Cl_2$, RT; 1 h; b) *n*-BuLi, $(CH_2O)_n$, anhydr. THF, $-20\ ^\circ C$ to RT, 3 h (72% over two steps); c) Phthalimide, DIAD, $PPh_3$, anhydr. THF, $0\ ^\circ C$ to RT, 1 h (90%); d) aq. HCl (1% v/v), EtOH, $40\ ^\circ C$, 4 h (97%); e) $NH(Cbz)_2$, DIAD, $PPh_3$, anhydr. THF, $0\ ^\circ C$ to RT, 1 h (45%); f) $B_{10}H_{14}$, bmim$^+$Cl$^-$, anhydr. toluene, $120\ ^\circ C$, 1.5 h (48% or $^{10}B_{10}H_{14}$, bmim$^+$Cl$^-$, anhydr. toluene, $120\ ^\circ C$, 1.5 h (53%); g) $H_2$, Pd/C 5 wt%, 1 N HCl, EtOH, RT, 16 h (**8**: 96%, $^{10}$**B-8**: 95%); h) Ar-NCO, *i*-$Pr_2$EtN, anhydr. THF, $40\ ^\circ C$, 2 h (**9a** 90%, **9b** 87%, $^{10}$**B-9b** 88%, **9c** 85%, $^{10}$**B-9c** 86%); i) *i*) $NaBH_4$, *i*-PrOH:$H_2O$ 4:1, RT, 3 h, *ii*) glacial $CH_3COOH$:conc. HCl:$H_2O$ 4:1:1, $80\ ^\circ C$, 2 h, *iii*) CHCl$_3$ (**10a** 90%, **10b** 99%, $^{10}$**B-10b** 92%, **10c** 85%, $^{10}$**B-10c**: 91%); l) $SO_2(NH_2)_2$, anhydr. 1,4-dioxane, reflux, 2 h (**CA-USF** 48%, **F-CA-USF** 55%, $^{10}$**B-F-CA-USF** 56%, **NO$_2$-CA-USF** 56%, $^{10}$**B-NO$_2$-CA-USF** 58%).

## 2.2. Determination of CA II and CA IX inhibition

It is reported that the zinc based mechanism responsible for $CO_2$ hydration is also responsible of esterase activity of CA II and CA IX [58, 59]. Therefore, the inhibition of CA II and CA IX enzymes can be indirectly screened employing a rapid colorimetric assay based on the use of 4-nitro-phenyl acetate (*p*NPA) as the substrate [60]. The hydrolysis of *p*NPA was spectrophotometrically followed by measuring the increase in the absorbance at 405 nm caused by the 4-nitrophenol (4-NP). The CA II and CA IX enzymes (5 μg/mL) were incubated with increasing concentration of *p*NPA substrate (0.2–10 mM) (Fig. S1 in ESI) [61]. The $V_{max}$ and $K_m$ calculated according to the Michaelis-Menten equation are reported in Table 1, and resulted in good agreement with the values reported in the literature by Uda and co-workers [61].

To determine the $IC_{50}$ (Fig. S2 in ESI), and the inhibition constant ($K_I$), CA II or CA IX (5 μg/mL) were pre-incubated with the different CA inhibitors **CA-USF**, **F-CA-USF**, **NO$_2$-CA-USF**, **CA-SF** at increasing concentrations respectively from 0.01 to 2 μM for CA II and from 0.001 to 100 μM for CA IX, in the presence of *p*NPA substrate (0.5 mM). The $K_I$ of the different compounds were compared with the commercially

available reference compound AZ (Table 2). Due to the low solubility of CA-USFs in aqueous solutions, the CA inhibitors were previously dissolved in DMSO and then mixed with an excess of 2-hydroxypropyl-β-cyclodextrin (HP-β-CD in PBS) in a 1:5 M ratio. $K_I$ were calculated by using the Cheng-Prusoff equation, as follows:

$$K_I = IC_{50}/(1 + [S]/K_m)$$

where [S] represents the *p*NPA concentration and $K_m$ the Michaelis-Menten constant reported in Table 1.

The results reported in Table 2 confirm that the introduction of a fluorine or nitro substituent on the aromatic group is fundamental to improve the inhibition of both enzymes. These results are in agreement with that obtained by Pacchiano et al. for compounds **II** and **III** [28]. Interestingly, both the reference inhibitor AZ (with and without HP-β-CD, Fig. S3) and the **NO$_2$-CA-USF** (+HP-β-CD) showed a higher inhibition of CA IX esterase activity with respect to the ubiquitous CA II. Moreover, as reported also for the precursor compound **III**, *i.e.* without the carborane, **NO$_2$-CA-USF**, was confirmed to be the most selective compound showing the highest inhibition of CA IX.

## 2.3. Cell viability assay (MTT)

The MTT assay, under normoxic conditions (5% $CO_2$, 37 °C), was then employed to evaluate the *in vitro* cytotoxicity of HP-β-CD inclusion complexes of the newly synthesised **CA-USFs** (in a molar ratio of 1:5 CA inhibitor:HP-β-CD) and of **CA-SF** as a reference, following the protocol reported by Azzi et al. [63] Two mesothelioma cell lines have been considered in this study: AB22 (murine) and ZL34 (human). As shown in Table 3, all the **CA-USFs** exhibited a greater toxicity with respect to **CA-SF** on AB22 cell line. Interestingly, the nitro-derivative, **NO$_2$-CA-USF**, showed a higher toxicity on both mesothelioma cell lines and a low value of $EC_{50}$ for AB22 cells (Table 3 entry 1) as expected

**Table 1**
Esterase activity of CA II and CA IX enzymes measured after incubation for 45 and 120 min, respectively.

| Enzyme | This work | | Reference values | |
|---|---|---|---|---|
| | $K_m$ [mM] | $V_{max}$ [nmol/min] | $K_m$ [mM] [62] | $V_{max}$ [nmol/min] [62] |
| CA II (45 min) | $4.2 \pm 1.3$ | $1.0 \pm 0.14$ | 3.2 | $1.002 \pm 0.14$ |
| CA IX (120 min) | $7.5 \pm 1.6$ | $0.36 \pm 0.04$ | $12.05 \pm 1.59$ [64] | $0.67 \pm 0.04$ [64] |

**Table 2**
IC$_{50}$ and $K_I$ of CA II and CA IX for the different CAIX inhibitors.

| Inhibitor | CA II | | CA IX | |
|---|---|---|---|---|
| | IC$_{50}$ [μM] | $K_I$ [μM] | IC$_{50}$ [μM] | $K_I$ [μM] |
| CA-USF + HP-β-CD | 1.280 | 1.2 ± 0.5 | 8.0 ± 5.0 | 5.3 ± 2.1 |
| F-CA-USF + HP-β-CD | 0.223 ± 0.015 | 0.197 ± 0.01 | 2.3 ± 0.6 | 2.15 ± 0.6 |
| NO$_2$-CA-USF + HP-β-CD | 0.241 ± 0.02 | 0.215 ± 0.01 | 0.0047 ± 0.003 | 0.0044 ± 0.0035 |
| CA-SF + HP-β-CD | 0.067 ± 0.009 | 0.0588 ± 0.002 | 0.7 ± 0.5 | 0.65 ± 0.15 |
| AZ + HP-β-CD | 0.08 ± 0.0079 | 0.0679 ± 0.003 | 0.014 ± 0.01 | 0.013 ± 0.007 |
| AZ | 0.085 ± 0.003 | 0.072 ± 0.002 | 0.006 ± 0.002 | 0.006 ± 0.003 |

**Table 3**
Inhibitory effect of different CA IX inhibitors against AB22 and ZL34.

| Entry | | EC$_{50}$ [μM] | | | | | |
|---|---|---|---|---|---|---|---|
| | | CA-USF + HP-βCD | F-CA-USF + HP-βCD | NO$_2$-CA-USF + HP-βCD | CA-SF + HP-βCD | AZ + HP-βCD | AZ |
| 1 | AB22 | 245.9 ± 6.8 | 257.9 ± 20 | 82 ± 3.1 | >300 | >500 | >500 |
| 2 | ZL34 | >300 | >300 | 237.8 ± 35.8 | >300 | >500 | >500 |

on the basis of their higher CA IX expression [57]. This result emphasises the critical role of the carborane in enhancing the hydrophobic interactions of biologically active compounds with their receptors, thus increasing their *in vivo* stability and bioavailability. In addition, the data reported in Table 3, on one hand, demonstrated the roles of the nitro group and the sulfonamide moiety as the key players in controlling the inhibitory potency, thus improving the affinity of the molecule for the target enzyme CA IX. On the other hand, the addition of the fluorine group did not significantly improve the cytotoxicity of the **F-CA-USF** derivative on AB22 cell lines compared to the reference ureido-molecule **CA-USF**. Moreover, the cytotoxic effect of AZ was not affected by the addition of HP-β-CD (Fig. S4).

### 2.4. Cell uptake experiment

In order to assess if the amount of boron taken up by AB22 (murine) and ZL34 (human) mesothelioma cells was sufficient to perform an efficient BNCT treatment, cells were incubated for 24 h at 37 °C, 5% CO$_2$ with increasing concentrations of the most promising ureido compounds **F-CA-USF** and **NO$_2$-CA-USF** as the HP-β-CD inclusion complexes (in a molar ratio of 1:5 CA inhibitor:HP-β-CD). After the incubation, the cells were washed with ice-cold PBS, collected, and the internalised boron content was quantified using ICP-MS and normalised to the total protein content of the cells. Fig. 2A revealed higher B mol/mg of total cell proteins on both AB22 and ZL34 cells incubated with compound **NO$_2$-CA-USF**/HP-β-CD compared to those incubated with compound **F-CA-USF**/HP-β-CD.

The μg/g of boron internalised in cells were determined by ICP-MS analysis by means of a calibration curve as described in the ESI. The μg of boron per g of tissue were thus calculated considering that in the case of epithelial tumours with an average diameter of 15–20 μm, a density of about 10$^8$ cells for cm$^3$ is a reasonable number for an effective BNCT treatment [64]. Furthermore, the μg/g of boron internalised by AB22 were higher than ZL34 for both CA inhibitors (Fig. 2B). Therefore, AB22 cells, previously treated with $^{10}$B-F- or $^{10}$B-NO$_2$-CA-USFs, were exposed to thermal neutron irradiation in the University of Pavia's
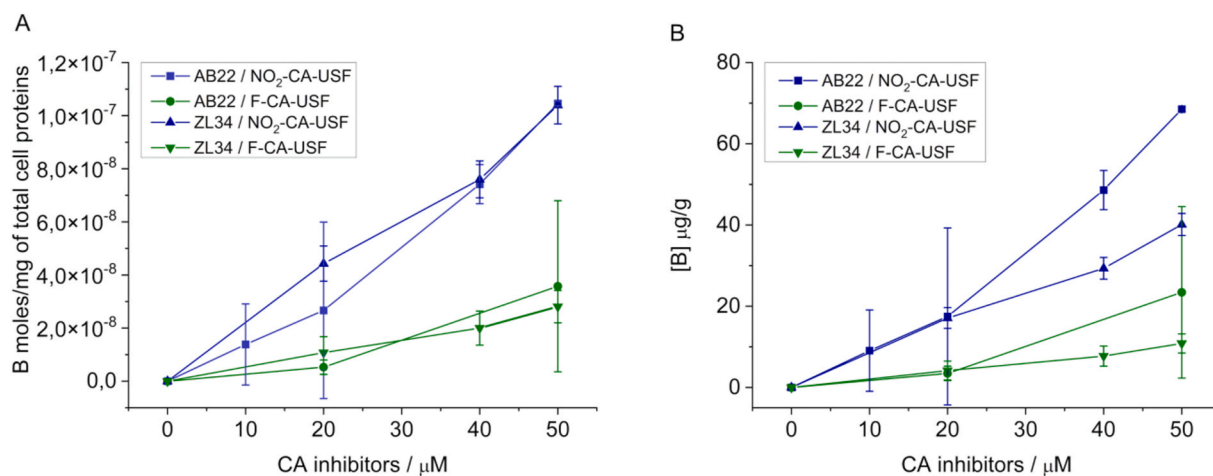


**Fig. 2.** Boron uptake on AB22 and ZL34 cells incubated in the presence of increasing concentration of **NO$_2$-CA-USF** and **F-CA-USF** (for 24 h at 37 °C). Boron concentration is expressed as moles of B per mg of cell proteins (A) or as μg B per g of tissue or ppm (B).

TRIGA Mark II reactor. The results were crucial to determine whether the binary therapy, *i.e.* based on both CA IX inhibition and BNCT, could improve the treatment outcomes compared to a single therapy.

### 2.5. In vitro BNCT treatment of AB22 cells

AB22 cells were incubated for 24 h with HP-β-CD inclusion complexes of $^{10}$B-NO$_2$-CA-USF or $^{10}$B-F-CA-USF (in a 1:5 M ratio) at a concentration of 50 μM, to reach the maximum intracellular boron content. The neutron-irradiated groups (CTRL IRR, $^{10}$B-F-CA-USF IRR and $^{10}$B-NO$_2$-CA-USF IRR) were exposed for 15 min to the radiation field of the thermal column of the TRIGA Mark II reactor at a 30 kW power. Fig. 3A compares the viability (%) of the cells treated with $^{10}$B-F-CA-USF and $^{10}$B-NO$_2$-CA-USF after 24 h from neutron irradiation with non-irradiated cells (CTRL). For the latter, the cell viability was set at 100%. Twenty-four hours was a too short interval to observe the additional effect of BNCT with respect to the CA IX inhibition only. In fact, Fig. 3A shows that the remaining viable cells were almost the same after the administration of $^{10}$B-NO$_2$-CA-USF and $^{10}$B-F-CA-USF with or without irradiation. In addition, a not negligible toxic effect of neutron irradiation (30%) has also been measured on cells irradiated in the absence of boron. Interestingly, as displayed in Fig. 3B, a marked inhibition of proliferation after irradiation was observed only for AB22 cells treated with $^{10}$B-F-CA-USF and $^{10}$B-NO$_2$-CA-USF. Interestingly, twenty days after neutron irradiation, re-growth was observed only for the cells treated with $^{10}$B-F-CA-USF. In fact, CA IX inhibition alone was not sufficient to obtain a complete hamper of cell proliferation but only a delay of about 8 days after neutron irradiation. These results support the idea that only $^{10}$B-NO$_2$-CA-USF efficiently prevents the AB22

proliferation of tumour cells when used alone and completely inhibits tumour recurrence in combination with the BNCT treatment. Finally, to confirm the proliferation assay results, a clonogenic assay was performed 16 days after neutron irradiation. Results are shown in Fig. 3C. Only cells that underwent BNCT treatment displayed a lower colony-forming capability, only few colonies were observed in $^{10}$B-F-CA-USF treated and irradiated cells, whereas in the case of irradiated AB22 treated with $^{10}$B-NO$_2$-CA-USF compound, no colony formation was noticed.

### 2.6. Combination of CA IX inhibition and BNCT treatment in a mouse model of mesothelioma

Murine mesothelioma cell line AB22 was selected for further *in vivo* studies due to its superior boron accumulation. In order to assess the additive therapeutic effect of BNCT and CA IX enzymatic inhibition, the syngeneic mouse model was prepared by subcutaneously implanting AB22 cells near the base of the neck of Balb/c mice (n = 20). After 6 days from the inoculation, the AB22 tumours reached a volume of roughly 60 ± 20 mm$^3$, thus the mice were divided into six groups: 1) control (CTRL, n = 4); 2) neutron irradiated control (CTRL IRR, n = 3); 3) treated with $^{10}$B-F-CA-USF ($^{10}$B-F-CA-USF, n = 3); 4) treated with $^{10}$B-NO$_2$-CA-USF ($^{10}$B-NO$_2$-CA-USF, n = 3); 5) treated with $^{10}$B-F-CA-USF and irradiated with neutrons ($^{10}$B-F-CA-USF IRR, n = 3); 6) treated with $^{10}$B-NO$_2$-CA-USF and irradiated with neutrons ($^{10}$B-NO$_2$-CA-USF IRR, n = 4). In particular, groups 3–6 received 7 doses of 8.15 mg/kg of boron, administered in the tail, as an inclusion complex CA-inhibitor/cyclodextrin-polymer (MW = 125,000) (CA-inhibitor:poly-β-CD unit, molar ratio of 1:3,6), along 14 days as described in the treatment plan
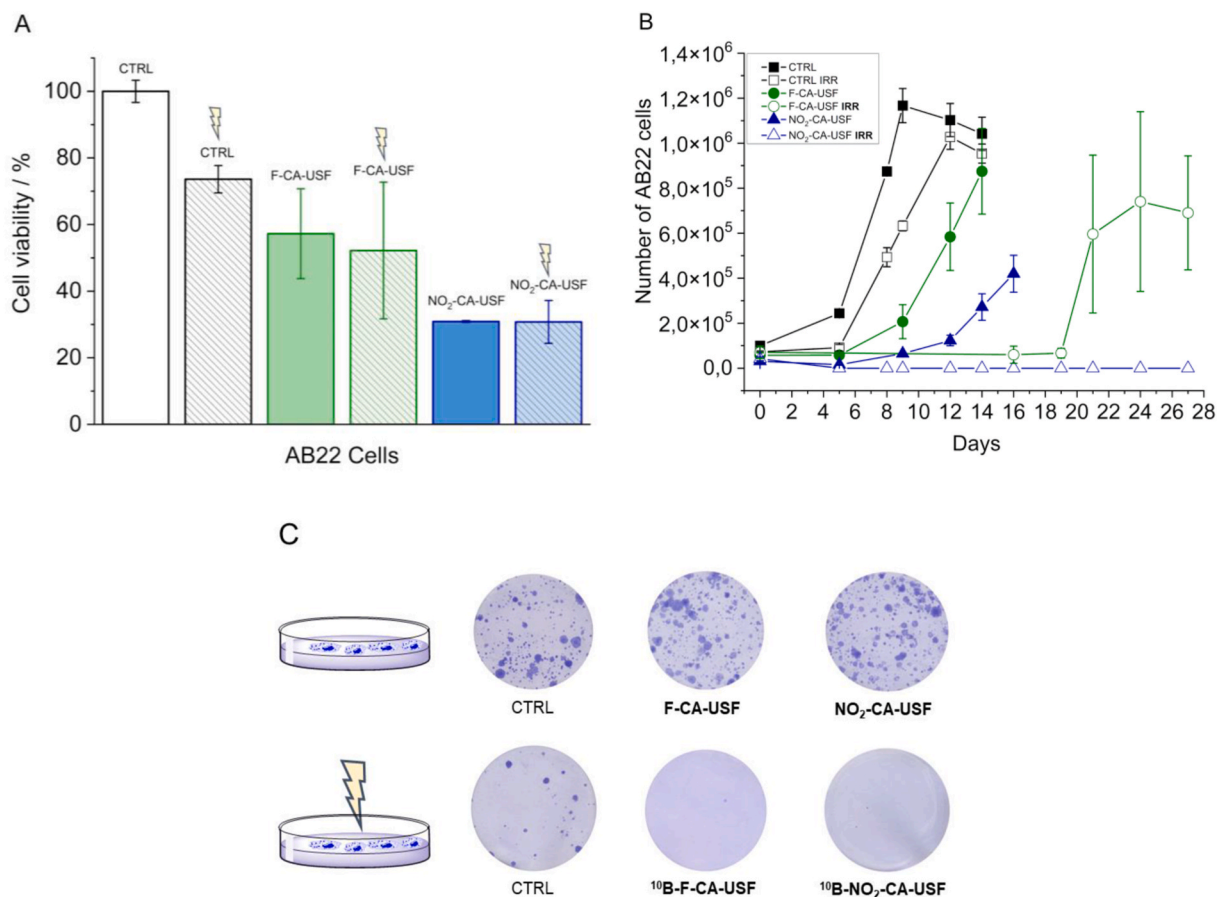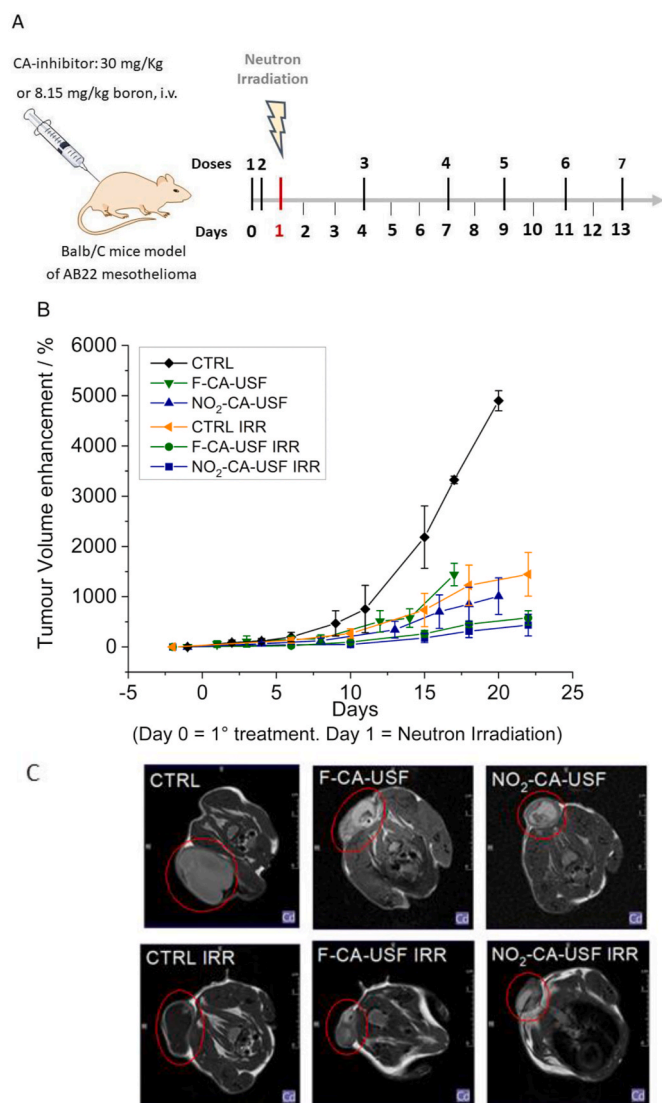


**Fig. 3.** (A) Number of viable cells 24 h after neutron irradiation of $^{10}$B F-CA-USF/HP-β-CD and $^{10}$B NO$_2$-CA-USF/HP-β-CD. (B) Effect of the irradiation after $^{10}$B F-CA-USF/HP-β-CD and $^{10}$B NO$_2$-CA-USF/HP-β-CD treatment on breast AB22 (proliferation rate of cells surviving to irradiation). (C) Clonogenic assay performed 16 days after neutron irradiation. Error bars indicate the SD.

**Fig. 4.** A) Schematic representation of the experimental plan; B) Tumour-growth evaluation performed after $^{10}$**B F-CA-USF** and $^{10}$**B NO$_2$-CA-USF** treatment. The graph shows the tumour volume increase measured by MRI on control mice, $^{10}$**B F-CA-USF** and $^{10}$**B NO$_2$-CA-USF** treated mice, irradiated control mice and irradiated and treated mice. Error bars indicate the SD; C) representative T2 weighted MRI of all the mice groups acquired at 17/18 days after neutron irradiation.

(Fig. 4A). The cyclodextrin-polymer was used instead of HP-β-CD monomer because of its high solubility in aqueous media. In addition, the significantly higher molecular weight increases its selective extravasation into tumour tissue and reduces clearance. In fact, drug formulations, in particular those with sizes >10 nm, have the ability to escape fast glomerular filtration, effectively extravasate inflammatory tissues with defective endothelium, such as cancer and persist for a long time in extracellular environments. Moreover, cyclodextrin access to membrane-bound cholesterol is restricted by the dimensions and structure of the polymeric material which is not able to disrupt the plasma membrane and may offer a more secure therapeutic alternative than the monomeric form [65–67]. The $^{10}$**B-F-CA-USF** and $^{10}$**B-NO$_2$-CA-USF** irradiated groups (5 and 6) received the first two doses 22 and 16 h before the 15 min irradiation in the thermal column of the TRIGA Mark II reactor (250 kW power). After BNCT, all the mice groups were monitored by Magnetic Resonance Imaging (MRI) and the tumour volume was measured for the following 22 days by analysing T$_2$

weighted MRI images acquired at 7 T. Fig. 4B shows the tumour volume enhancement (%) calculated from MRI images acquired at 7 T until the end of the experiment. Fig. 4C displays representative T$_2$ weighted MRI of all the mice groups acquired at 17/18 days after neutron irradiation.

Mice tumour treated with $^{10}$**B-NO$_2$-CA-USF** or $^{10}$**B-F-CA-USF** exhibits a size reduction in comparison to the un-treated control mice with a significantly higher effect in combination with BNCT. Interestingly, in the absence of BNCT, the slowing down of the tumour growth is more pronounced in mice treated with $^{10}$**B-NO$_2$-CA-USF** with respect to $^{10}$**B-F-CA-USF**, thus confirming the *in vitro* results (Fig. 3). Another key feature of this treatment is the employment of a lower dose, 30 mg/kg for $^{10}$**B-NO$_2$-CA-USF** and $^{10}$**B-F-CA-USF**, that is about 30%, than the reference compound SLC-0001 (100 mg/kg) used for the *in vivo* treatment of an orthotopic, syngeneic model of CA IX-positive breast cancer [22].

The additive BNCT effect is evident and statistically significant in both treated mice groups (p = 0.012 and 0.023 for $^{10}$**B-F-CA-USF** and $^{10}$**B-NO$_2$-CA-USF**, respectively) but no significant differences in tumour growth were observed between the two BNCT groups treated with the $^{10}$**B-NO$_2$-CA-USF** and $^{10}$**B-F-CA-USF** under these conditions. This similar efficacy can be due to the low administered boron concentration along with the occurrence of a high tumour response to the neutron irradiation alone. In fact, the irradiated control group curve was lower with respect to the not irradiated one. To confirm this hypothesis, a new strategy has to be carried out to improve the solubility and the delivery of **CA-USFs** adducts. Finally, no significant weight reduction (Fig. S5, ESI) was observed for any of the treated animals also after neutron irradiation, thus demonstrating that the compounds are well-tolerated *in vivo* at a therapeutically active dose.

## 3. Conclusions

In this paper, new multivalent agents for the treatment of mesothelioma have been successfully exploited, with the aim of combining BNCT and CAs inhibition as therapeutic strategies. An efficient synthetic protocol allowed carboranyl ureidobenzenesulfamides substituted with a fluorine atom and a nitro group (**NO$_2$-CA-USF** and **F-CA-USF**) to be efficiently obtained in eleven steps. *In vitro* BNCT experiments on AB22 murine and ZL34 human mesothelioma cells demonstrated the efficacy of combining the inhibition of CA IX with the BNCT treatment. A complete hamper of cell proliferation was in fact observed, especially for **NO$_2$-CA-USF**. *In vivo* experiments were also carried out on a AB 22 mouse model of mesothelioma. Treated mice tumour showed a size reduction compared to untreated control mice with a significantly higher effect in combination with BNCT. In both *in vitro* and *in vivo* experiments, the CA inhibitors were administered as inclusion complexes of β-CD thus increasing their solubility in aqueous media, their bioavailability and at the same time, reducing their toxicity. In fact, **CA-USFs** demonstrated to be *in vivo* well tolerated at a therapeutic dose. The therapeutic potential of this treatment could be extended to other cancers that exhibit elevated CA IX activity, including melanoma, glioma, and breast cancer. Moreover, other CA-USFs derivatives will be prepared, including differently substituted aryl or heteroaryl rings, in order to rationalise the structure-activity relationship. Another strategy that can be pursued to increase the water solubility of these derivatives is the transformation of the highly lipophilic closo-into nido-carborane, that contains nine boron atoms and with a negative charge. In fact, nido-Carborane-based compounds, as Na + salts or as internal salts, are generally more soluble in water than the corresponding closo-derivatives [68].

# 4. Experimental part

## 4.1. Chemistry

### 4.1.1. General

Flasks and all equipment used for the generation and reaction of moisture-sensitive compounds were dried by electric heat gun under $N_2$. All commercially available reagents and solvents were used as received. Anhydrous solvents were purchased by Sigma-Aldrich and Acros. THF was distilled from $LiAlH_4$ then benzophenone ketyl and $CH_2Cl_2$ from $CaH_2$ prior to use. *n*-BuLi (2.5 M in hexanes) was obtained from Sigma-Aldrich. Decaborane was bought from KATCHEM spol. s. r. o. Products were purified by preparative column chromatography on Macherey-Nagel silica gel for flash chromatography, 0,04–0,063 mm/230–400 mesh. When specified, silica gel is deactivated with 1% of $Et_3N$. Reactions were monitored by TLC using Silica gel on TLC-PET foils Merck, layer thickness 0.2 mm, medium pore diameter 60 Å. Carboranes and their derivatives were visualised on TLC plates using a 5% $PdCl_2$ aqueous solution in HCl. $^1H$ NMR spectra were recorded at NMR Jeol ECZR 600 MHz, $^{13}C$ NMR spectra at 150 MHz and 100 MHz, $^{11}B$ NMR spectra at 192.5 MHz, $^{19}F$ NMR spectra at 564.8 MHz in CDCl₃, CD₃OD or acetone-$d_6$. Data were reported as follows: chemical shifts in ppm from tetramethylsilane as the internal standard, integration, multiplicity (s = singlet, d = doublet, t = triplet, q = quartet, dd = double-doublet, m = multiplet, br = broad), coupling constants (Hz), and assignment. $^{13}C$ NMR, $^{11}B$ NMR and $^{19}F$ spectra were measured with complete proton decoupling. DEPT experiments were carried out with a DEPT 135 sequence. Chemical shifts were reported in ppm from the residual solvent as an internal standard. The MS flow-injection analyses were run on a "Orbitrap Fusion Tribrid high resolution" mass spectrometer (Thermo Scientific, Rodano, Italy), equipped with an atmospheric pressure interface and an ESI ion source. Samples were analyzed by flow injection at a 15 μL min⁻¹ flow rate. The tuning parameters adopted for the ESI source were: ion spray voltage 3.8 kV and tube lens voltage 60%. The ion transfer tube and the vaporizer temperature were maintained at 300 °C and 60 °C, respectively. Sheath and auxiliary gases were set at 5 and 1 arb (arbitrary unit), respectively. The mass accuracy of the recorded ions (*vs.* the calculated ones) was <5 mmu (milli-mass units). Analyses were run using full MS at 150–2000 *m/z* in the positive ion mode. IR spectra were recorded on a PerkinElmer BX FT-IR. Melting point analyses were carried out with a SMP3 Bibbi Stuart Scientific system. MR image was acquired on a Bruker Avance Neo 300 MHz spectrometer (7 T) equipped with a Micro 2.5 microimaging probe (Bruker BioSpin, Ettlingen, Germany). Inductively coupled plasma mass spectrometry (ICP-MS) (Element-2; Thermo-Finnigan, Rodano (MI), Italy) was used to measure the amount of boron in cell samples. Intermediates from **1** to **7** were synthesised following the reported procedures [69]. Compound **6** was subjected to a pre-chromatography on silica using DCM/MeOH 100:1 as the eluant to remove the hydrazide by-product, then purified by column chromatography using EP/Et₂O 50:50 as the eluant.

## 4.2. Procedures

### 4.2.1. $^{10}B$-enriched-C-(N-(1,3-dioxoisoindolin-2-yl))methyl-C′-2-(N,N-dibenzyloxycarbonyl)aminoethyl-o-carborane ($^{10}B$-7)

In a dried heavy wall tube with screw cap under nitrogen atmosphere, bmim⁺Cl⁻ (0.6 eq., 0.45 mmol, 0.079 g) was dried at 100 °C under high vacuum to remove water traces. Then, 2-(5-(*N,N*-dibenzyloxycarbonyl)aminopent-2-yn-1-yl)isoindoline-1,3-dione **6** (1.0 eq., 0.75 mmol, 0.37 g) and $^{10}B$-enriched-decaborane (1.0 eq., 0.75 mmol, 0.086 g) were suspended in a biphasic mixture of bmim⁺Cl⁻ and 4 mL of anhydrous toluene. The mixture was vigorously stirred at 120 °C for 1.5 h. After cooling to room temperature, the solvent was evaporated under reduced pressure and the crude was purified on flash silica gel (PE:Et₂O 50:50) to yield $^{10}B$-7 as a white solid (0.24 g, 53%). $^1H$ NMR (600 MHz, CDCl₃, Me₄Si) δ 7.91–7.87 (2H, m, Phth-*H*), 7.82–7.79 (2H, m, Phth-*H*),

7.36–7.32 (4H, m, NHC(O)OCH₂Ar–*H*), 7.29–7.23 (6H, m, NHC(O)OCH₂Ar–*H*), 5.24 (2H, s, NHC(O)OCH₂Ar), 4.00 (2H, s, PhthNCH₂C-BH), 3.99–3.93 (2H, m, CH₂CH₂NHC(O)OCH₂Ar), 2.85–2.79 (2H, m, CH₂CH₂NHC(O)OCH₂Ar), 2.54–1.75 (10H, br, B₁₀H₁₀). $^{13}C$ NMR (150 MHz, CDCl₃, Me₄Si) δ 167.0 (Cq), 152.6 (Cq), 134.8 (CH), 131.5 (Cq), 128.8 (CH), 128.8 (CH), 128.6 (CH), 124.0 (CH), 78.1 (Cq), 76.5 (Cq), 69.4 (CH₂), 45.6 (CH₂), 39.4 (CH₂), 32.9 (CH₂). Rf: 0.26 (CH₂Cl₂:MeOH 200:1), UV and PdCl₂ active. Mp: 47.1–49.5 °C. $\nu_{max}$ (neat)/cm⁻¹ 2590, 1755, 1721, 1392, 1356, 1292, 1204, 1110, 1090, 962, 910, 718, 697. HRMS for $C_{29}H_{34}{}^{10}B_{10}N_2O_6$ Calcd. 629,3603 [M + Na]⁺, Found: 629,3617 [M + Na]⁺.

### 4.2.2. C-(N-(1,3-dioxoisoindolin-2-yl))methyl-C′-2-aminoethyl-o-carborane hydrochloric salt (8•HCl) [69]

To a stirred solution of *C*-(*N*-(1,3-dioxoisoindolin-2-yl))methyl-*C′*-2-(*N,N*-dibenzyloxycarbonyl)aminoethyl-o-carborane **7** (1.0 eq., 0.5 mmol, 0.33 g) in 10 mL of a EtOH:AcOEt 1:1 mixture, Pd/C (10 wt%, 0.033 g) and aqueous 1 N HCl (1.1 eq., 0.6 mmol, 0.60 mL) were added. The reaction vessel was evacuated and backfilled with hydrogen, then the suspension was vigorously stirred over night at room temperature under a hydrogen atmosphere (1 atm). The reaction was filtered and the solvent was evaporated under reduced pressure to afford **8•HCl** as a white solid (0.20 g, 96%), which was used in the following step without further purification. $^1H$ NMR (600 MHz; MeOD) δ 7.98–7.93 (2H, m, Phth-*H*), 7.92–7.88 (2H, m, Phth-*H*), 4.50 (2H, s, PhthNCH₂), 3.30–3.24 (2H, m, CH₂CH₂NH₃⁺), 3.06–3.01 (2H, m, CH₂CH₂NH₃⁺), 2.78–1.60 (10H, br, B-*H*). $^{13}C$ NMR (150 MHz, CDCl₃, Me₄Si) δ 168.8 (Cq), 136.3 (CH), 132.7 (Cq), 124.9 (CH), 79.7 (Cq), 78.9 (Cq), 41.0 (CH₂), 39.7 (CH₂), 32.9 (CH₂). $^{11}B$ NMR (192.5 MHz, MeOD) δ −5.90, −6.59, −10.67, −11.45, −12.73. Rf: 0.11 (CH₂Cl₂:MeOH 95:5), UV and PdCl₂ active. Mp: 220.2–223.0 °C (degradation, brown solid). $\nu_{max}$ (neat)/cm⁻¹ 2958, 2884, 2583, 1774, 1712, 1395, 1355, 1126, 716. HRMS for $C_{13}H_{22}B_{10}N_2O_2$ Calcd. 349.2685 [M + H]⁺, Found: 349.2673 [M + H]⁺.

### 4.2.3. $^{10}B$-enriched-C-(N-(1,3-dioxoisoindolin-2-yl))methyl-C′-2-aminoethyl-o-carborane hydrochloric salt ($^{10}B$-8•HCl) [69]

To a stirred solution of $^{10}B$-enriched-*C*-(*N*-(1,3-dioxoisoindolin-2-yl))methyl-*C′*-2-(*N,N*-dibenzyloxycarbonyl)aminoethyl-o-carborane $^{10}B$-7 (1.0 eq., 0.41 mmol, 0.25 g) in 10 mL of a EtOH:AcOEt 1:1 mixture, Pd/C (10 wt%, 0.025 g) and aqueous 1 N HCl (1.1 eq., 0.49 mmol, 0.49 mL) were added. The reaction vessel was evacuated and backfilled with hydrogen, then the suspension was vigorously stirred over night at room temperature under a hydrogen atmosphere (1 atm). The reaction was filtered and the solvent was evaporated under reduced pressure to afford $^{10}B$-8•HCl as a white solid (0.13 g, 95%), which was used in the following step without further purification. $^1H$ NMR (600 MHz, MeOD) δ 7.97–7.93 (2H, m, Phth-*H*), 7.92–7.88 (2H, m, Phth-*H*), 4.50 (2H, s, PhthNCH₂C-BH), 3.30–3.25 (2H, m, CH₂CH₂NH₃⁺), 3.06–3.01 (2H, m, CH₂CH₂NH₃⁺), 2.80–1.65 (10H, br, B₁₀H₁₀). $^{13}C$ NMR (150 MHz, MeOD) δ 168.8 (Cq), 136.3 (CH), 132.7 (Cq), 124.9 (CH), 79.6 (Cq), 78.9 (Cq), 41.0 (CH₂), 39.7 (CH₂), 32.9 (CH₂). Rf: 0,12 (CH₂Cl₂:MeOH 95:5), UV and PdCl₂ active. Mp: 162 °C (degradation, brown solid). $\nu_{max}$ (neat)/cm⁻¹ 2586, 1772, 1712, 1398, 1355, 1126, 716. HRMS for $C_{13}H_{22}{}^{10}B_{10}N_2O_2$ Calcd. 339,3048 [M + H]⁺, Found: 339,3052 [M + H]⁺.

## 4.3. General procedure for the substitued aryl ureas

In a dried round bottom flask under nitrogen atmosphere, *C′*-2-aminoethyl-o-carborane hydrochloric salt (1.0 eq.) was suspended in freshly distilled THF. The appropriate isocyanate (1.1 eq.) and DIPEA (1.1 eq.) were added dropwise. The mixture was stirred at 40 °C until total disappearance of the reagent spot on TLC plate was observed (about 2 h). The solvent was evaporated under reduced pressure and the crude was purified by column chromatography on flash silica gel.

### 4.3.1. C-(N-(1,3-dioxoisoindolin-2-yl))methyl-C′-2-(phenylcarbamoyl) aminoethyl-o-carborane (9a)

According to the described general procedure, C-(N-(1,3-dioxoisoindolin-2-yl))methyl-C′-2-aminoethyl-o-carborane hydrochloric salt **8•HCl** (0.25 mmol, 0.094 g) was reacted with phenyl isocyanate (0.27 mmol, 0.032 g, 0.029 mL), and DIPEA (0.27 mmol, 0.035 g, 0.047 mL) in 5 mL of freshly distilled THF to obtain a crude oil, purified on flash silica gel (CH$_2$Cl$_2$:MeOH 98:2) to yield **9a** as a white solid (0.11 g, 93%). $^1$H NMR (600 MHz, CDCl$_3$, Me$_4$Si) $\delta$ 7.85–7.81 (2H, m, Phth-*H*), 7.77–7.73 (2H, m, Phth-*H*), 7.40 (1H, s, CON*H*Ar), 7.28–7.21 (4H, m, CONHAr-*H*), 7.01 (1H, t, $J = 7.2$ Hz, CONHAr-*H*), 5.67 (1H, t, $J = 5.9$ Hz, N*H*CONHAr), 4.32 (2H, s, PhthNC*H*$_2$C-BH), 3.41 (2H, q, $J = 6.5$ Hz, CH$_2$C*H*$_2$NH), 2.74 (2H, t, $J = 7.6$ Hz, C*H*$_2$CH$_2$NH), 2.70–1.58 (10H, br, B$_{10}$*H*$_{10}$). $^{13}$C NMR (150 MHz, CDCl$_3$, Me$_4$Si) $\delta$ 167.3 (Cq), 156.2 (Cq), 138.4 (Cq), 134.9 (CH), 131.4 (Cq), 129.4 (CH), 124.1 (CH), 121.0 (CH), 79.1 (Cq), 40.0 (CH$_2$), 39.6 (CH$_2$), 34.9 (CH$_2$). $^{11}$B NMR (192.5 MHz, CDCl$_3$, Me$_4$Si) $\delta$ −5.08, −10.31, −11.84. Rf: 0,41 (CH$_2$Cl$_2$:MeOH 95:5), UV and PdCl$_2$ active. Mp: 90 °C (degradation, yellow gummy solid). $\nu_{max}$ (neat)/cm$^{-1}$ 3337, 2581, 1722, 1647, 1534, 1395, 1355, 1250, 907, 716. HRMS for C$_{20}$H$_{27}$B$_{10}$N$_3$O$_3$ Calcd. 488,2948 [M + Na]$^+$, Found: 488,2952 [M + Na]$^+$.

### 4.3.2. C-(N-(1,3-dioxoisoindolin-2-yl))methyl-C′-2-(4′-fluorophenylcarbamoyl)aminoethyl-o-carborane (9b)

According to the described general procedure, C-(N-(1,3-dioxoisoindolin-2-yl))methyl-C′-2-aminoethyl-o-carborane hydrochloric salt **8•HCl** (0.70 mmol, 0,27 g) was reacted with 4-fluorophenyl isocyanate (0,77 mmol, 0,11 g, 0,088 mL), and DIPEA (0,77 mmol, 0,10 g, 0,13 mL) in 5 mL of freshly distilled THF to obtain a crude oil, purified on flash silica gel (CH$_2$Cl$_2$:MeOH 98:2) to yield **9b** as a white solid (0,3 g, 87%). $^1$H NMR (600 MHz, CDCl$_3$, Me$_4$Si) $\delta$ 7.91–7.88 (2H, m, Phth-*H*), 7.82–7.78 (2H, m, Phth-*H*), 7.29–7.25 (2H, m, NHCC*H*CHCF), 7.05–7.00 (2H, m, NHCCHC*H*CF), 6.27 (1H, brs, N*H*CONH), 5.00 (1H, brs, NHCON*H*), 4.45 (2H, s, PhthNC*H*$_2$C-BH), 3.54 (2H, t, $J = 7.4$ Hz, CH$_2$C*H*$_2$NH), 2.85 (2H, t, $J = 7.4$ C*H*$_2$CH$_2$NH), 2.76–1.75 (10H, br, B$_{10}$*H*$_{10}$). $^{13}$C NMR (150 MHz, CDCl$_3$, Me$_4$Si) $\delta$ 167.3 (Cq), 159.5 (d, $J_{C\text{-}F}$ = 243 Hz, Cq), 156,2 (Cq), 134.9 (CH), 134.1 (CH), 131.3 (Cq), 124.1 (CH), 123.2 (d, $^3J_{C\text{-}F}$ = 8 Hz, CH), 116.0 (d, $^2J_{C\text{-}F}$ = 22 Hz, CH), 79.0 (Cq), 77.2 (Cq), 39.9 (CH$_2$), 39.7 (CH$_2$), 35.0 (CH$_2$). $^{11}$B NMR (192.5 MHz, CDCl$_3$, Me$_4$Si) $\delta$ −4.66, −10.29, −12.01. $^{19}$F NMR (564.7 MHz, CDCl$_3$, Me$_4$Si) $\delta$ −117.9. Rf: 0,35 (CH$_2$Cl$_2$:MeOH 98:2), UV and PdCl$_2$ active. Mp: 102 °C (degradation, yellow gummy solid). $\nu_{max}$ (neat)/cm$^{-1}$ 3337, 2579, 1777, 1720, 1644, 1560, 1507, 1395, 1354, 1214, 833, 716. HRMS for C$_{20}$H$_{26}$B$_{10}$FN$_3$O$_3$ Calcd. 506,2854 [M + Na]$^+$, Found: 506,2861 [M + Na]$^+$.

### 4.3.3. $^{10}$B-enriched-C-(N-(1,3-dioxoisoindolin-2-yl))methyl-C′-2-(4′-fluorophenylcarbamoyl)aminoethyl-o-carborane ($^{10}$B–9b)

According to the described general procedure, $^{10}$B-enriched-C-(N-(1,3-dioxoisoindolin-2-yl))methyl-C′-2-aminoethyl-o-carborane hydrochloric salt **$^{10}$B-8•HCl** (0,15 mmol, 0,051 g) was reacted with 4-fluorophenyl isocyanate (0,17 mmol, 0,023 g, 0,019 mL), and DIPEA (0,17 mmol, 0,021 g, 0,030 mL) in 5 mL of freshly distilled THF to obtain a crude oil, purified on flash silica gel (CH$_2$Cl$_2$:MeOH 97:3) to yield **$^{10}$B-9b** as a white solid (0,063 g, 88%). $^1$H NMR (600 MHz, CDCl$_3$, Me$_4$Si) $\delta$ 7.89–7.84 (2H, m, Phth-*H*), 7.80–7.76 (2H, m, Phth-*H*), 7.25–7.21 (2H, m, NHCC*H*CHCF), 6.99–6.94 (2H, m, NHCCHC*H*CF), 4.39 (2H, s, PhthNC*H*$_2$C-BH), 3.49 (2H, t, $J = 7.3$ Hz, CH$_2$C*H*$_2$NH), 2.80 (2H, t, $J = 7.6$ C*H*$_2$CH$_2$NH), 2.61–1.78 (10H, br, B$_{10}$*H*$_{10}$). $^{13}$C NMR (150 MHz, CDCl$_3$, Me$_4$Si) $\delta$ 167.4 (Cq), 159.7 (d, $J_{C\text{-}F}$ = 243 Hz, Cq), 156,2 (Cq), 135.0 (CH), 133.9 (CH), 131.3 (Cq), 124.1 (CH), 123.7 (d, $^3J_{C\text{-}F}$ = 7 Hz, CH), 116.1 (d, $^2J_{C\text{-}F}$ = 23 Hz, CH), 79.1 (Cq), 77.3 (Cq), 39.9 (CH$_2$), 39.8 (CH$_2$), 35.0 (CH$_2$). $^{19}$F NMR (564.7 MHz, CDCl$_3$, Me$_4$Si) $\delta$ −117.6. Rf: 0,40 (CH$_2$Cl$_2$:MeOH 97:3), UV and PdCl$_2$ active. Mp: 101 °C (degradation, yellow gummy solid). $\nu_{max}$ (neat)/cm$^{-1}$ 3337, 2592, 1777, 1723, 1646, 1562, 1508, 1396, 1356, 1216, 834, 717. HRMS for C$_{20}$H$_{26}$$^{10}$B$_{10}$FN$_3$O$_3$ Calcd. 498,3144 [M + Na]$^+$, Found: 498,3153 [M + Na]$^+$.

### 4.3.4. C-(N-(1,3-dioxoisoindolin-2-yl))methyl-C′-2-(3′-nitrophenylcarbamoyl)aminoethyl-o-carborane (9c)

According to the described general procedure, C-(N-(1,3-dioxoisoindolin-2-yl))methyl-C′-2-aminoethyl-o-carborane hydrochloric salt **8•HCl** (0,70 mmol, 0,27 g) was reacted with 3-nitrophenyl isocyanate (0,77 mmol, 0.13 g), and DIPEA (0,77 mmol, 0,10 g, 0,13 mL) in 5 mL of freshly distilled THF to obtain a crude solid, purified on flash silica gel (CH$_2$Cl$_2$:MeOH 97:3) to yield **9c** as a white solid (0,32 g, 87%). $^1$H NMR (600 MHz, acetone-$d_6$) $\delta$ 8.67 (1H, brs, NHCON*H*), 8.58 (1H, t, $J = 2.3$ Hz, C-C*H*-C-NO$_2$), 7.96–7.88 (4H, m, Phth-*H*), 7.76 (2H, dddd, $J = 17.0$, 8.2, 2.1, 0.7 Hz, C-CH-C*H*-CH-C-NO$_2$ and C-CH-CH-C*H*-C-NO$_2$), 7.48 (1H, t, $J = 8.2$ Hz, C-C*H*-CH-CH-C-NO$_2$), 6.34 (1H, t, $J = 5.7$ Hz, N*H*CONH), 4.57 (2H, s, PhthNC*H*$_2$C-BH), 3.58 (2H, dt, $J = 7.8$, 6.0 Hz, CH$_2$C*H*$_2$NH), 2.97 (2H, t, $J = 7.9$ Hz, C*H*$_2$CH$_2$NH), 2.80–1.56 (10H, br, B$_{10}$*H*$_{10}$). $^{13}$C NMR (150 MHz, acetone-$d_6$) $\delta$ 168.0 (Cq), 155.8 (Cq), 149.5 (Cq), 142.6 (Cq), 135.8 (CH), 132.3 (Cq), 130.5 (CH), 124.6 (CH), 124.5 (CH), 116.8 (CH), 113.2 (CH), 80.6 (Cq), 78.9 (Cq), 40.8 (CH$_2$), 40.2 (CH$_2$), 35.2 (CH$_2$). $^{11}$B NMR (192.5 MHz, acetone-$d_6$) $\delta$ −5.09, −6.00, −10.75, −11.76. Rf: 0,55 (CH$_2$Cl$_2$:MeOH 95:5), UV and PdCl$_2$ active. Mp: 209.6–210.8 °C. $\nu_{max}$ (neat)/cm$^{-1}$ 3376, 2578, 1778, 1721, 1697, 1523, 1349, 1247, 716. HRMS for C$_{20}$H$_{26}$B$_{10}$N$_4$O$_5$ Calcd. 549,2538 [M + K]$^+$, Found: 549,2547 [M + K]$^+$.

### 4.3.5. $^{10}$B-enriched-C-(N-(1,3-dioxoisoindolin-2-yl))methyl-C′-2-(3′-nitrophenylcarbamoyl)aminoethyl-o-carborane ($^{10}$B-9c)

According to the described general procedure, $^{10}$B-enriched-C-(N-(1,3-dioxoisoindolin-2-yl))methyl-C′-2-aminoethyl-o-carborane hydrochloric salt **$^{10}$B-8•HCl** (0,15 mmol, 0,051 g) was reacted with 3-nitrophenyl isocyanate (0,17 mmol, 0.027 g), and DIPEA (0,17 mmol, 0,021 g, 0,029 mL) in 5 mL of freshly distilled THF to obtain a crude solid, purified on flash silica gel (CH$_2$Cl$_2$:MeOH 97:3) to yield **$^{10}$B-9c** as a white solid (0,065 g, 86%). $^1$H NMR (600 MHz, acetone-$d_6$) $\delta$ 8.65 (1H, brs, NHCON*H*), 8.60 (1H, t, $J = 2.3$ Hz, C-C*H*-C-NO$_2$), 7.97–7.91 (4H, m, Phth-*H*), 7.78 (2H, dddd, $J = 17.9$, 8.3, 2.2, 0.9 Hz, C-CH-C*H*-CH-C-NO$_2$ and C-CH-CH-C*H*-C-NO$_2$), 7.50 (1H, t, $J = 8.2$ Hz, C-C*H*-CH-CH-C-NO$_2$), 6.32 (1H, t, $J = 5.7$ Hz, N*H*CONH), 4.58 (2H, s, PhthNC*H*$_2$C-BH), 3.61–3.55 (2H, m, CH$_2$C*H*$_2$NH), 3.00–2.95 (2H, m, C*H*$_2$CH$_2$NH), 2.70–1.70 (10H, br, B$_{10}$*H*$_{10}$). $^{13}$C NMR (150 MHz, CDCl$_3$, Me$_4$Si) $\delta$ 168.0 (Cq), 155.8 (Cq), 149.6 (Cq), 142.7 (Cq), 135.8 (CH), 132.4 (Cq), 130.6 (CH), 124.6 (CH), 124.5 (CH), 116.8 (CH), 113.2 (CH), 80.6 (Cq), 79.1 (Cq), 40.8 (CH$_2$), 40.2 (CH$_2$), 35.3 (CH$_2$). Rf: 0,42 (CH$_2$Cl$_2$:MeOH 97:3), UV and PdCl$_2$ active. Mp: 208.4–211.9 °C. $\nu_{max}$ (neat)/cm$^{-1}$ 3376, 2584, 1777, 1720, 1698, 1522, 1350, 1246, 716. HRMS for C$_{20}$H$_{26}$$^{10}$B$_{10}$N$_4$O$_5$ Calcd. 541,2828 [M + K]$^+$, Found: 541,2840 [M + K]$^+$.

### 4.4. General procedure for the phthaloyl group removal [70]

In a round bottom flask, the appropriate C-(N-(1,3-dioxoisoindolin-2-yl))methyl-o-carborane (1.0 eq.) was suspended in a mixture of i-PrOH:H$_2$O 4:1. NaBH$_4$ (5.0 eq.) was added and the reaction was stirred at room temperature until total disappearance of the reagent spot on TLC plate was observed (about 2 h). The solvent was removed under reduced pressure, then the crude was partitioned in H$_2$O (20 mL) and AcOEt (20 mL). The organic phase was separated and the aqueous layer was extracted with AcOEt (2 × 10 mL). The combined organic phases were dried over anhydrous Na$_2$SO$_4$ and evaporated under reduced pressure. The crude was then dissolved in a glacial AcOH:H$_2$O:37% v/v HCl 4:1:1 mixture and heated at 80 °C for 2 h. The solvent was removed under reduced pressure and the residue was sonicated with few mL of CHCl$_3$. The product was recovered by filtration and washing with few mL of CHCl$_3$.

### 4.4.1. C-aminomethyl-C′-2-(phenylcarbamoyl)aminoethyl-o-carborane hydrochloric salt (10a•HCl)

According to the described general procedure, *C*-(*N*-(1,3-dioxoisoindolin-2-yl))methyl-*C′*-2-(phenylcarbamoyl)aminoethyl-*o*-carborane **9a** (0.19 mmol, 0.090 g) was reacted with NaBH₄ (0.97 mmol, 0.037 g) in 10 mL of *i*-PrOH:H₂O 4:1. The crude solid obtained after extraction was dissolved in 12 mL of a glacial AcOH:H₂O:37% v/v HCl 4:1:1 mixture. The treatment with CHCl₃ afforded **10a•HCl** as a white solid (0.063 g, 99%). $^1$H NMR (600 MHz, MeOD) $\delta$ 7.35 (2H, d, *J* = 7.6 Hz, CONHAr-*H*), 7.25 (2H, t, *J* = 8.1 Hz, CONHAr-*H*), 6.99 (1H, t, *J* = 7.6 Hz, CONHAr-*H*), 4.02 (2H, s, C$_{cage}$C*H₂*NH₃⁺), 3.39–3.34 (2H, m, CH₂C*H₂*NH), 2.61–2.56 (2H, m, C*H₂*CH₂NH), 2.83–1.74 (10H, br, B₁₀*H*₁₀). $^{13}$C NMR (150 MHz, MeOD) $\delta$ 158.3 (Cq), 140.6 (Cq), 129.8 (CH), 123.8 (CH), 120.4 (CH), 80.3 (Cq), 75.8 (Cq), 42.8 (CH₂), 40.4 (CH₂), 35.4 (CH₂). $^{11}$B NMR (192.5 MHz, CDCl₃, Me₄Si) $\delta$ −4.20, −5.35, −10.47, −11.87. Rf: 0,44 (CH₂Cl₂:MeOH 90:10), UV and PdCl₂ active. Mp: 143 °C (degradation, white gummy solid). $\nu_{max}$ (neat)/cm$^{-1}$ 2950, 2879, 2595, 1638, 1500, 1476, 1449, 755. HRMS for C₁₂H₂₅B₁₀N₃O Calcd. 336,3074 [M]⁺, Found: 336,3077 [M]⁺.

### 4.4.2. C-aminomethyl-C′-2-(4′-fluorophenylcarbamoyl)aminoethyl-o-carborane hydrochloric salt (10b•HCl)

According to the described general procedure, *C*-(*N*-(1,3-dioxoisoindolin-2-yl))methyl-*C′*-2-(4′-fluorophenylcarbamoyl)aminoethyl-*o*-carborane **9b** (0,59 mmol, 0,28 g) was reacted with NaBH₄ (2,93 mmol, 0,11 g) in 15 mL of *i*-PrOH:H₂O 4:1. The crude solid obtained after extraction was dissolved in 18 mL of a glacial AcOH:H₂O:37% v/v HCl 4:1:1 mixture. The treatment with CHCl₃ afforded **10b•HCl** as a white solid (0,21 g, 99%). $^1$H NMR (600 MHz, MeOD) $\delta$ 7.34 (2H, dd, *J* = 9.0, 4.9 Hz, NHCCHC*H*CF), 7.00 (2H, t, *J* = 8.8 Hz, NHCC*H*CHCF), 4.01 (2H, s, C$_{cage}$C*H₂*NH₃⁺), 3.35 (2H, t, *J* = 7.9 Hz, CH₂C*H₂*NH), 2.58 (2H, t, *J* = 7.6 Hz, C*H₂*CH₂NH), 2.76–1.75 (10H, br, B₁₀*H*₁₀). $^{13}$C NMR (150 MHz, MeOD) $\delta$ 160.0 (d, *J*$_{C-F}$ = 239 Hz, Cq), 158,3 (Cq), 136.8 (Cq), 122.2 (d, $^3$*J*$_{C-F}$ = 8.2 Hz, CH), 116.2 (d, $^2$*J*$_{C-F}$ = 22 Hz, CH), 80.2 (Cq), 75.8 (Cq), 42.8 (CH₂), 40.4 (CH₂), 35.4 (CH₂). $^{11}$B NMR (192.5 MHz, MeOD) $\delta$ −4.19, −5.31, −10.49, −11.90. $^{19}$F NMR (564.7 MHz, MeOD) $\delta$ −122.7. Rf: 0,19 (CH₂Cl₂:MeOH 95:5), UV and PdCl₂ active. Mp: 148 °C (degradation, yellow gummy solid). $\nu_{max}$ (neat)/cm$^{-1}$ 3329, 2867, 2588, 1641, 1508, 1220, 833. HRMS for C₁₂H₂₄B₁₀FN₃O Calcd. 354,2979 [M]⁺, Found: 354,2982 [M]⁺.

### 4.4.3. $^{10}$B-enriched-C-aminomethyl-C′-2-(4′-fluorophenylcarbamoyl)aminoethyl-o-carborane hydrochloric salt ($^{10}$B–10b•HCl)

According to the described general procedure, $^{10}$B-enriched-*C*-(*N*-(1,3-dioxoisoindolin-2-yl))methyl-*C′*-2-(4′-fluorophenylcarbamoyl)aminoethyl-*o*-carborane $^{10}$**B-9b** (0,11 mmol, 0,054 g) was reacted with NaBH₄ (0,57 mmol, 0,022 g) in 5 mL of *i*-PrOH:H₂O 4:1. The crude solid obtained after extraction was dissolved in 12 mL of a glacial AcOH:H₂O:37% v/v HCl 4:1:1 mixture. The treatment with CHCl₃ afforded $^{10}$**B-10b•HCl** as a white solid (0,035 g, 92%). $^1$H NMR (600 MHz, MeOD) $\delta$ 7.37–7.32 (2H, m, NHCCHC*H*CF), 7.02–6.97 (2H, m, NHCC*H*CHCF), 4.01 (2H, s, C$_{cage}$C*H₂*NH), 3.39–3.34 (2H, m, CH₂C*H₂*NH), 2.61–2.56 (2H, m, C*H₂*CH₂NH), 2.76–1.75 (10H, br, B₁₀*H*₁₀). $^{13}$C NMR (150 MHz, MeOD) $\delta$ 159.2 (Cq), 158,3 (Cq), 136.8 (Cq), 122.3 (d, $^3$*J*$_{C-F}$ = 7.6 Hz, CH), 116.2 (d, $^2$*J*$_{C-F}$ = 23 Hz, CH), 80.3 (Cq), 75.8 (Cq), 42.8 (CH₂), 40.4 (CH₂), 35.4 (CH₂). $^{19}$F NMR (564.7 MHz, MeOD) $\delta$ −121.35. Rf: 0,44 (CH₂Cl₂:MeOH 90:10), UV and PdCl₂ active. Mp: 146 °C (degradation, yellow gummy solid). $\nu_{max}$ (neat)/cm$^{-1}$ 2600, 1642, 1509, 1220, 833. HRMS for C₁₂H₂₄B₁₀FN₃O Calcd. 346,3270 [M + H]⁺, Found: 346,3277 [M + H]⁺.

### 4.4.4. C-aminomethyl-C′-2-(3-nitrophenylcarbamoyl)aminoethyl-o-carborane hydrochloric salt (10c•HCl)

According to the described general procedure, *C*-(*N*-(1,3-dioxoisoindolin-2-yl))methyl-*C′*-2-(3′-nitrophenylcarbamoyl)aminoethyl-*o*-carborane **9c** (0.58 mmol, 0.3 g) was reacted with NaBH₄ (2.91 mmol,

0.11 g) in 15 mL of *i*-PrOH:H₂O 4:1. The crude solid obtained after extraction was dissolved in 18 mL of a glacial AcOH:H₂O:37% v/v HCl 4:1:1 mixture. The treatment with CHCl₃ afforded **10c•HCl** as a yellow solid (0.23 g, 96%). $^1$H NMR (600 MHz, MeOD) $\delta$ 8.53 (1H, t, *J* = 2.2 Hz, C-C*H*-C-NO₂), 7.83 (1H, ddd, *J* = 8.1, 2.2, 0.9 Hz, C-CH-CH-C*H*-C-NO₂), 7.60 (1H, dd, *J* = 8.1, 2.2 Hz, C-CH-C*H*-CH-C-NO₂), 7.47 (1H, t, *J* = 8.1 Hz, C-C*H*-CH-CH-C-NO₂), 4.03 (2H, s, C$_{cage}$C*H₂*NH), 3.39 (2H, t, *J* = 7.9 Hz, CH₂C*H₂*NH), 2.62 (2H, t, *J* = 8.2 Hz, C*H₂*CH₂NH), 2.91–1.65 (10H, br, B₁₀*H*₁₀). $^{13}$C NMR (150 MHz, MeOD) $\delta$ 157.6 (Cq), 150.0 (Cq), 142.4 (Cq), 130.7 (CH), 125.2 (CH), 117.6 (CH), 113.9 (CH), 80.2 (Cq), 75.6 (Cq), 42.7 (CH₂), 40.3 (CH₂), 35.3 (CH₂). $^{11}$B NMR (192.5 MHz, MeOD) $\delta$ −4.28, −5.44, −10.52, −12.00. Rf: 0,49 (CH₂Cl₂:MeOH 90:10), UV and PdCl₂ active. Mp: 184 °C (degradation, yellow gummy solid). $\nu_{max}$ (neat)/cm$^{-1}$ 3359, 2589, 1652, 1526, 1470, 1437, 1350, 737. HRMS for C₁₂H₂₄B₁₀N₄O₃ Calcd. 381,2924 [M]⁺, Found: 381,2927 [M]⁺.

### 4.4.5. $^{10}$B-enriched-C-aminomethyl-C′-2-(3-nitrophenylcarbamoyl)aminoethyl-o-carborane hydrochloric salt ($^{10}$B-10c•HCl)

According to the described general procedure, $^{10}$B-enriched-*C*-(*N*-(1,3-dioxoisoindolin-2-yl))methyl-*C′*-2-(3′-nitrophenylcarbamoyl)aminoethyl-*o*-carborane $^{10}$**B-9c** (0.098 mmol, 0.049 g) was reacted with NaBH₄ (0.49 mmol, 0.018 g) in 5 mL of *i*-PrOH:H₂O 4:1. The crude solid obtained after extraction was dissolved in 6 mL of a glacial AcOH:H₂O:37% v/v HCl 4:1:1 mixture. The treatment with CHCl₃ afforded $^{10}$**B-10c•HCl** as a yellow solid (0.033 g, 91%). $^1$H NMR (600 MHz, MeOD) $\delta$ 8.53 (1H, t, *J* = 2.1 Hz, C-C*H*-C-NO₂), 7.83 (1H, ddd, *J* = 7.9, 2.2, 0.9 Hz, C-CH-CH-C*H*-C-NO₂), 7.60 (1H, dd, *J* = 7.9, 2.1 Hz, C-CH-C*H*-CH-C-NO₂), 7.47 (1H, t, *J* = 8.3 Hz, C-C*H*-CH-CH-C-NO₂), 4.03 (2H, s, C$_{cage}$C*H₂*NH), 3.42–3.36 (2H, m, CH₂C*H₂*NH), 2.66–2.58 (2H, m, C*H₂*CH₂NH), 2.75–1.80 (10H, br, B₁₀*H*₁₀). $^{13}$C NMR (150 MHz, MeOD) $\delta$ 157.7 (Cq), 150.1 (Cq), 142.4 (Cq), 130.8 (CH), 125.2 (CH), 117.7 (CH), 114.0 (CH), 80.3 (Cq), 75.6 (Cq), 42.8 (CH₂), 40.4 (CH₂), 35.3 (CH₂). Rf: 0,47 (CH₂Cl₂:MeOH 90:10), UV and PdCl₂ active. Mp: 183 °C (degradation, yellow gummy solid). $\nu_{max}$ (neat)/cm$^{-1}$ 2599, 1648, 1526, 1470, 1436, 1350, 737. HRMS for C₁₂H₂₄$^{10}$B₁₀N₄O₃ Calcd. 373,3215 [M + H]⁺, Found: 373,3222 [M + H]⁺.

## 4.5. General procedure for the sulfamidic group installation [57]

In a dried round bottom flask under nitrogen atmosphere, the appropriate *C*-aminomethyl-*o*-carborane (1.0 eq.) was suspended in anhydrous 1,4-dioxane. Sulfamide (5.0 eq.) was added and the mixture was stirred at reflux until total disappearance of the reagent spot on TLC plate was observed (about 2 h). The solvent was evaporated under reduced pressure and the crude was dissolved in AcOEt (20 mL) and a 10% aqueous KHSO₄ (20 mL). The organic phase was separated and the aqueous layer was extracted with AcOEt (2 × 10 mL). The combined organic phases were dried over anhydrous Na₂SO₄ and evaporated under reduced pressure. The crude was then purified by column chromatography on flash silica gel.

### 4.5.1. C-(sulfamoylamino)methyl-C′-2-(phenylcarbamoyl)aminoethyl-o-carborane (CA-USF)

According to the described general procedure, *C*-aminomethyl-*C′*-2-(phenylcarbamoyl)aminoethyl-*o*-carborane hydrochloric salt **10a•HCl** (0.17 mmol, 0.056 g) was reacted with sulfamide (0.84 mmol, 0.080 g) in 5 mL of anhydrous 1,4-dioxane. The crude solid obtained after extraction was purified on flash silica gel (CH₂Cl₂:MeOH 95:5) to yield **CA-USF** as a white solid (0.034 g, 48%). $^1$H NMR (600 MHz, acetone-$d_6$) $\delta$ 8.17 (1H, brs, NHCON*H*), 7.47–7.41 (2H, m, NHAr-*H*), 7.26–7.20 (2H, m, NHAr-*H*), 6.98–6.92 (1H, tt, *J* = 7.4, 1.1 Hz NHAr-*H*), 6.82 (1H, t, *J* = 7.7 Hz, CH₂N*H*SO₂NH₂), 6.34 (2H, s, CH₂NHSO₂N*H₂*), 6.09 (1H, s, N*H*Ar-H), 4.02 (2H, d, *J* = 7.6 Hz, C*H₂*NHSO₂NH₂), 3.44–3.38 (2H, m, CH₂C*H₂*NH), 2.69–2.64 (2H, m, C*H₂*CH₂NH), 2.90–1.58 (10H, br, B₁₀*H*₁₀). $^{13}$C NMR (150 MHz, acetone-$d_6$) $\delta$ 156.5 (Cq), 141.0 (Cq), 129.5 (CH), 122.8 (CH), 119.4 (CH), 80.5 (Cq), 79.1 (Cq), 46.9 (CH₂),

40.1 (CH$_2$), 35.1 (CH$_2$). $^{11}$B NMR (192.5 MHz, acetone-*d$_6$*) δ −5.68, −11.66. Rf: 0,19 (CH$_2$Cl$_2$:MeOH 95:5), UV and PdCl$_2$ active. Mp: 78.4–82.2 °C. $\nu_{max}$ (neat)/cm$^{-1}$ 3355, 2583, 1652, 1552, 1499, 1441, 1315, 1253, 1158, 755, 730. HRMS for C$_{12}$H$_{26}$B$_{10}$N$_4$O$_3$S Calcd. 453,2360 [M + K]$^+$, Found: 453,2362 [M + K]$^+$.

### 4.5.2. *C-(sulfamoylamino)methyl-C'-2-(4'-fluorophenylcarbamoyl) aminoethyl-o-carborane (F-CA-USF)*

According to the described general procedure, *C*-aminomethyl-*C'*-2-(4'-fluorophenylcarbamoyl)aminoethyl-*o*-carborane hydrochloric salt **10b•HCl** (0.57 mmol, 0.20 g) was reacted with sulfamide (2.87 mmol, 0.28 g) in 15 mL of anhydrous 1,4-dioxane. The crude solid obtained after extraction was purified on flash silica gel (CH$_2$Cl$_2$:MeOH 95:5) to yield **F-CA-USF** as a white solid (0.15 g, 55%). $^1$H NMR (600 MHz, acetone-*d$_6$*) δ 8.22 (1H, brs, NHCON*H*), 7.45 (2H, dd, *J* = 9.1, 4,8 Hz, NHCC*H*CHC*H*CF), 7.00 (2H, t, *J* = 8.8 Hz, NHCC*H*CHCF), 6.81 (1H, t, *J* = 7.2 Hz, CH$_2$N*H*SO$_2$NH$_2$), 6.32 (2H, s, CH$_2$NHSO$_2$N*H$_2$*), 6.10 (1H, s, N*H*CCHCHCF), 4.01 (2H, d, *J* = 7.7 Hz, C*H$_2$*NHSO$_2$NH$_2$), 3.44–3.39 (2H, m, CH$_2$C*H$_2$*NH), 2.69–2.63 (2H, m, C*H$_2$*CH$_2$NH), 2.90–1.65 (10H, br, B$_{10}$*H$_{10}$*). $^{13}$C NMR (150 MHz, acetone-*d$_6$*) δ 159.0 (d, *J$_{C-F}$* = 238 Hz, Cq), 156,6 (Cq), 137.3 (CH), 121.2 (d, $^3$*J$_{C-F}$* = 6.9 Hz, CH), 115.9 (d, $^2$*J$_{C-F}$* = 22 Hz, CH), 80.5 (Cq), 79.1 (Cq), 46.9 (CH$_2$), 40.1 (CH$_2$), 35.0 (CH$_2$). $^{11}$B NMR (192.5 MHz, CDCl$_3$, Me$_4$Si) δ −5.68, −11.61. $^{19}$F NMR (564.7 MHz, MeOD) δ −123.03. Rf: 0,70 (pure AcOEt), UV and PdCl$_2$ active. Mp: 68 °C (degradation, yellow gummy solid). $\nu_{max}$ (neat)/cm$^{-1}$ 3305, 2584, 1649, 1557, 1509, 1339, 1157, 835. HRMS for C$_{12}$H$_{25}$B$_{10}$FN$_4$O$_3$S Calcd. 471,2266 [M + K]$^+$, Found: 471,2268 [M + K]$^+$.

### 4.5.3. $^{10}$B-enriched-C-(sulfamoylamino)methyl-C'-2-(4'-fluorophenylcarbamoyl)aminoethyl-o-carborane ($^{10}$B-F-CA-USF)

According to the described general procedure, $^{10}$B-enriched-*C*-aminomethyl-*C'*-2-(4'-fluorophenylcarbamoyl)aminoethyl-*o*-carborane hydrochloric salt $^{10}$**B-10b•HCl** (0.084 mmol, 0.029 g) was reacted with sulfamide (0.42 mmol, 0.040 g) in 5 mL of anhydrous 1,4-dioxane. The crude solid obtained after extraction was purified on flash silica gel (CH$_2$Cl$_2$:MeOH 95:5) to yield $^{10}$**B-F-CA-USF** as a white solid (0.020 g, 56%). $^1$H NMR (600 MHz, acetone-*d$_6$*) δ 8.22 (1H, brs, NHCON*H*), 7.48–7.40 (2H, NHCC*H*CHC*H*CF), 7.03–6.96 (2H, m, NHCC*H*CHCF), 6.82 (1H, t, *J* = 7.8 Hz, CH$_2$N*H*SO$_2$NH$_2$), 6.33 (2H, s, CH$_2$NHSO$_2$N*H$_2$*), 6.09 (1H, s, N*H*CCHCHCF), 4.00 (2H, d, *J* = 8.1 Hz, C*H$_2$*NHSO$_2$NH$_2$), 3.44–3.38 (2H, m, CH$_2$C*H$_2$*NH), 2.68–2.63 (2H, m, C*H$_2$*CH$_2$NH), 2.75–1.78 (10H, br, B$_{10}$*H$_{10}$*). $^{13}$C NMR (150 MHz, acetone-*d$_6$*) δ 158.9 (d, *J$_{C-F}$* = 238 Hz, Cq), 156,6 (Cq), 137.2 (CH), 121.2 (d, $^3$*J$_{C-F}$* = 7.3 Hz, CH), 115.9 (d, $^2$*J$_{C-F}$* = 22 Hz, CH), 80.5 (Cq), 79.1 (Cq), 46.9 (CH$_2$), 40.1 (CH$_2$), 35.0 (CH$_2$). $^{19}$F NMR (564.7 MHz, MeOD) δ −123.02. Rf: 0,68 (pure AcOEt), UV and PdCl$_2$ active. Mp: 69 °C (degradation, yellow gummy solid). $\nu_{max}$ (neat)/cm$^{-1}$ 3315, 2586, 1649, 1555, 1509, 1340, 1157, 836. HRMS for C$_{12}$H$_{25}$$^{10}$B$_{10}$FN$_4$O$_3$S Calcd. 463,2557 [M + K]$^+$, Found: 463,2562 [M + K]$^+$.

### 4.5.4. *C-(sulfamoylamino)methyl-C'-2-(3'-nitrophenylcarbamoyl) aminoethyl-o-carborane (NO$_2$-CA-USF)*

According to the described general procedure, *C*-aminomethyl-*C'*-2-(3'-nitrophenylcarbamoyl)aminoethyl-*o*-carborane hydrochloric salt **10c•HCl** (0.58 mmol, 0.22 g) was reacted with sulfamide (2.91 mmol, 0.28 g) in 15 mL of anhydrous 1,4-dioxane. The crude solid obtained after extraction was purified on flash silica gel (CH$_2$Cl$_2$:MeOH 95:5) to yield **NO$_2$-CA-USF** as a yellow solid (0.15 g, 56%). $^1$H NMR (600 MHz, acetone-*d$_6$*) δ 8.68 (1H, brs, NHCON*H*), 8.52 (1H, t, *J* = 2.2 Hz, C-C*H*-C-NO$_2$), 7.80 (1H, ddd, *J* = 8.2, 2.3, 0.9 Hz, C-CH-CH-C*H*-C-NO$_2$), 7.75 (1H, ddd, *J* = 8.2, 2.2, 0.9 Hz, C-CH-C*H*-CH-C-NO$_2$), 7.51 (1H, t, *J* = 8.2 Hz, C-C*H*-CH-CH-C-NO$_2$), 6.80 (1H, t, *J* = 7.7 Hz, CH$_2$N*H*SO$_2$NH$_2$), 6.30 (2H, s, CH$_2$NHSO$_2$N*H$_2$*), 6.25 (1H, t, *J* = 6.0 Hz, N*H*CONH), 4.01 (2H, d, *J* = 7.7 Hz, C*H$_2$*NHSO$_2$NH$_2$), 3.50–3.42 (2H, m, CH$_2$C*H$_2$*NH), 2.72–2.66 (2H, m, C*H$_2$*CH$_2$NH), 2.85–1.58 (10H, br, B$_{10}$*H$_{10}$*). $^{13}$C NMR (150 MHz, acetone-*d$_6$*) δ 156.0 (Cq), 149.6 (Cq), 142.4 (Cq), 130.6 (CH), 124.8

(CH), 117.0 (CH), 113.3 (CH), 80.5 (Cq), 79.0 (Cq), 46.9 (CH$_2$), 40.1 (CH$_2$), 34.9 (CH$_2$). $^{11}$B NMR (192.5 MHz, acetone-*d$_6$*) δ −5.59, −11.54. Rf: 0,55 (pure AcOEt), UV and PdCl$_2$ active. Mp: 84.6–87.1 °C. $\nu_{max}$ (neat)/cm$^{-1}$ 3282, 2578, 1686, 1547, 1523, 1345, 1252, 1156, 736. HRMS for C$_{12}$H$_{25}$B$_{10}$N$_5$O$_5$S Calcd. 498,2211 [M + K]$^+$, Found: 498,2212 [M + K]$^+$.

### 4.5.5. $^{10}$B-enriched-C-(sulsecamoylamino)methyl-C'-2-(3'-nitrophenylcarbamoyl)aminoethyl-o-carborane ($^{10}$B-NO$_2$-CA-USF)

According to the described general procedure, $^{10}$B-enriched-*C*-aminomethyl-*C'*-2-(3'-nitrophenylcarbamoyl)aminoethyl-*o*-carborane hydrochloric salt $^{10}$**B-10c•HCl** (0.078 mmol, 0.029 g) was reacted with sulfamide (0.39 mmol, 0.038 g) in 5 mL of anhydrous 1,4-dioxane. The crude solid obtained after extraction was purified on flash silica gel (CH$_2$Cl$_2$:MeOH 95:5) to yield $^{10}$**B-NO$_2$-CA-USF** as a yellow solid (0.020 g, 58%). $^1$H NMR (600 MHz, acetone-*d$_6$*) δ 8.68 (1H, brs, NHCON*H*), 8.52 (1H, t, *J* = 2.2 Hz, C-C*H*-C-NO$_2$), 7.80 (1H, ddd, *J* = 8.3, 2.2, 1.0 Hz, C-CH-CH-C*H*-C-NO$_2$), 7.76 (1H, ddd, *J* = 8.3, 2.2, 1.0 Hz, C-CH-C*H*-CH-C-NO$_2$), 7.51 (1H, t, *J* = 8.1 Hz, C-C*H*-CH-CH-C-NO$_2$), 6.80 (1H, t, *J* = 7.7 Hz, CH$_2$N*H*SO$_2$NH$_2$), 6.29 (2H, s, CH$_2$NHSO$_2$N*H$_2$*), 6.25 (1H, t, *J* = 5.5 Hz, N*H*CONH), 4.01 (2H, d, *J* = 7.6 Hz, C*H$_2$*NHSO$_2$NH$_2$), 3.49–3.43 (2H, m, CH$_2$C*H$_2$*NH), 2.72–2.66 (2H, m, C*H$_2$*CH$_2$NH), 2.80–1.75 (10H, br, B$_{10}$*H$_{10}$*). $^{13}$C NMR (150 MHz, acetone-*d$_6$*) δ 156.0 (Cq), 149.6 (Cq), 142.5 (Cq), 130.6 (CH), 124.8 (CH), 117.0 (CH), 113.3 (CH), 80.6 (Cq), 79.1 (Cq), 46.9 (CH$_2$), 40.1 (CH$_2$), 34.9 (CH$_2$). Rf: 0,53 (pure AcOEt), UV and PdCl$_2$ active. Mp: 82.9–85.2 °C. $\nu_{max}$ (neat)/cm$^{-1}$ 3370, 2593, 1686, 1548, 1526, 1348, 1254, 1160, 737. HRMS for C$_{12}$H$_{25}$$^{10}$B$_{10}$N$_5$O$_5$S Calcd. 490,2502 [M + K]$^+$, Found: 490,2507 [M + K]$^+$.

## 5. Biology

### 5.1. Determination of CA esterase activity

Recombinant human CA IX and bovine CA II enzymes, Acetazolamide (AZ) and *p*-nitrophenyl acetate (*p*NPA) were purchased from Sigma Aldrich. All the CA assay experiments were performed in 96-well flat-bottom plates, purchased from VWR International S.r.l. (Milano, Italy). The CA esterase activity was determined using an ester substrate (*p*NPA) which is hydrolysed in a chromophore 4-nitrophenol (4-NP). The released product can be easily quantified spectrophotometrically. In the presence of a CA specific inhibitor, the enzyme activity is blocked, which results in a decrease of absorbance. To measure the affinity of the *p*NPA substrate for the enzymes CA II and CA IX, *p*NPA (dissolved in acetone) was incubated at 0.2–10 mM in the presence of a fixed concentration of the enzyme CA II (5 μg/ml (166 nM)) or CA IX (5 μg/ml (119 nM)) in a final volume of 100 μl in a reaction mixture buffer (12.5 mM Tris, 75 mM NaCl, pH 7.5). The final percentage of acetone was 5% for [*p*NPA] ≤ 2 mM and 10% [*p*NPA] > 2 mM. Binding affinity was measured by monitoring, at room temperature, the formation of 4-NP at 405 nm, by GloMax® Discover Microplate Reader (Promega corporation, Milano, Italy) for 1 and 2 h for CAII and CAIX, respectively. In order to use the same conditions of the inhibition experiment (*vide infra*) the enzyme solutions were pre-incubated for 15 min at 25 °C and 1 h at 37 °C for CA II and CA IX, respectively. Data were analyzed by using OriginPro 8.5 software. The values for V$_{max}$, K$_m$, and the apparent K$_m$ (K$_m$ app) were determined utilising the Michaelis-Menten equation. The inhibition of CA II and CA IX esterase was measured by incubating CA II (5 μg/mL (166 nM)) or CA IX (5 μg/mL (119 nM)) with different CA inhibitors: CA-USF, F-CA-USF, NO$_2$-CA-USF, CA-SF and acetazolamide (AZ) (Sigma Aldrich) in a different range of concentrations (0.01–2 μM and 0.001–100 μM for CA II and CA IX, respectively) in the presence of *p*NPA substrate (0.5 mM) in 100 μL of final volume in a reaction mixture buffer (12.5 mM Tris, 75 mM NaCl, pH 7.5). The CA inhibitors were previously dissolved in DMSO (Sigma Aldrich) and then mixed with HP-β-CD (in PBS) in a molar ratio of 1:5 (CA inhibitor:HP-β−CD). The pre-incubation was performed at 25 °C for 15 min or at 37 °C for 1 h, for CA

II and CA IX, respectively. The esterase activity was measured by monitoring the production of 4-NP at 405 nm at regular intervals of 10 min for 180 min at room temperature. The esterase activity (%) in the presence or in the absence of the CA inhibitors was calculated through kinetic activity curves by plotting the absorbance (405 nm) on the Y-axis and time (minutes) on the X-axis and the $IC_{50}$ values were calculated by using OriginPro 8.5 software. The dissociation constant ($K_{diss}$) was calculated using the following formula:

$$K_{diss} = IC_{50} / (1 + \text{substrate concentration}) / K_m.$$

The percentage of CA inhibition was calculated by setting to 100% the esterase activity in the absence of inhibitors.

### 5.2. Cell lines

AB22 murine mesothelioma and ZL34 human mesothelioma cell lines were obtained from Sigma Aldrich. The AB22 cells were cultured in RPMI 1640 media supplemented with 25 mM Hepes (Lonza), 10% (v/v) Fetal Bovine Serum (FBS), and 2 mM of L-glutamine (Lonza). The ZL34 cells were cultured in DMEM-Ham's F12 (Lonza) containing 2.5 mM glutamine and supplemented with 15% (v/v) FBS. All media contained 100 U/mL penicillin and 100 U/mL streptomycin. All the cell lines were maintained at 37 °C in a 5% $CO_2$ incubator.

### 5.3. MTT

The MTT assay is utilised to measure the reduction of succinate dehydrogenase in metabolically active cell mitochondria, resulting in the formation of purple formazan crystals. Following the protocol outlined by Azzi et al. [63], the assay was conducted as follows: $6 \times 10^3$ and $1 \times 10^4$ cells per well were seeded in a 96-well microtiter plate for AB22 and ZL34 cell line, respectively. After 24 h at 37 °C and 5% $CO_2$, the cells were exposed to increasing concentrations, 0–0.3 mM, of compounds (stock solution in DMSO) CA-SF, CA-USF, F-CA-USF and $NO_2$-CA-USF previously incubated in the presence of hydroxypropyl β-cyclodextrin dissolved in PBS (HP-β−CD) in a molar ratio of 1:5 (CA inhibitor: HP-β−CD) to enhance their water solubility. The inclusion complexes CA inhibitor/HP-β−CD were incubated with AB22 and ZL34 for 24 h under normoxic conditions (at 37 °C and 5% $CO_2$). The concentration of DMSO in the cell medium did not exceed 0.5% (v/v) in all the conditions tested. After the incubation, the medium was removed, and each well was incubated with thiazolyl blue tetrazolium bromide (Sigma Aldrich) dissolved in the medium at a concentration of 0.45 mg/mL. The cells were then incubated for 4 h at 37 °C and 5% $CO_2$. Finally, the medium was removed and 150 μL of DMSO were added to each well to dissolve the formazan salt crystals produced because of live cell metabolism. The microplate was incubated at room temperature (RT) for 30 min and then, the absorbance was measured at 565 nm, using GloMax® Discover Microplate Reader (Promega corporation, Milano, Italy). Cell viability was determined as the percentage of dead cells observed in the treated samples relative to the non-treated control cells. The $EC_{50}$ values of each CA inhibitor were calculated by fitting the Dose Response MTT curve with a Origin 8.5 software using the equation:

$$y = A1 + (A2-A1)/(1 + 10^{((LOGx0-X) \times p)})$$

where A1 and A2 are bottom and top asymptote, respectively; LOGx0 and p are center and hill slope, respectively.

### 5.4. Cell uptake [59]

For *in vitro* uptake experiments, AB22 and ZL34 cells were seeded in 6 cm diameter dishes at the following densities: $7 \times 10^5$ and $1 \times 10^6$ cells, respectively. After 24 h at 37 °C, 5% $CO_2$ in a cell incubator, the cells were incubated for other 24 h with increasing concentrations of F-CA-USF and $NO_2$-CA-USF, preincubated with HP-β-CD as described

before. The concentration of DMSO in the cell medium was maintained under 0.5% (v/v) in all the conditions tested. At the end of the incubation, the cells were washed three times with 3 mL of ice-cold PBS and detached using a solution of 0.05% trypsin and 0.02% EDTA. Subsequently, all cell samples were transferred in Falcon tubes, re-suspended in 200 μL of PBS and sonicated at 30% power for 30 s in ice. Then, the protein content of each cell sample was evaluated by Bradford assay (BioRad) using bovine serum albumin as a standard. Finally, the boron content internalised by each cell sample was measured by ICP-MS (see below) and then normalised to its total protein content. The cell number was obtained from the mg of cell proteins measured by Bradford assay, using the calibration curve: [(mg protein)/(number of cells)]. From this calibration 1 mg of proteins of AB22 and ZL34 correspond to 1.65 and 2.8 million cells, respectively. From ICP-MS data, it was possible to calculate boron ppm by assuming a density of about $10^8$ cells for $cm^3$ in the case of epithelial tumours (with a diameter ranging 15–20 μm).

### 5.5. Cell irradiation

$7 \times 10^5$ AB22 cells were seeded in twelve T25 flasks. After 24 h, four flasks were incubated with 50 μM $^{10}$B-enriched-F-CA-USF/HP-β−CD and four flasks with 50 μM $^{10}$B-enriched–$NO_2$–CA-USF/HP-β−CD. The CA inhibitors, before the incubation with cells, were pre-incubated with HP-β−CD as described before. The remaining four flasks were used as control. After the incubation, cells were washed with PBS and their medium was renewed. Two of the four flasks incubated with $^{10}$B-enriched-F-CA-USF/HP-β−CD or $^{10}$B-enriched–$NO_2$–CA-USF/HP-β−CD and two flasks containing non-treated control cells were irradiated at 30 kW reactor power in the thermal column of the TRIGA Mark II reactor at the University of Pavia, Italy. At the end of the irradiation, the medium was removed, replaced with fresh medium, and all the flasks (included the non-irradiated) were placed in a humidified atmosphere of 5% $CO_2$ at 37 °C.

### 5.6. Proliferation and clonogenic assay [64]

The proliferation assay was carried out following the same procedure as described by Alberti et al. [58] The day after the irradiation, cells were detached using 0.05% trypsin and 0.02% EDTA, and a trypan blue exclusion test was performed to assess cell viability. Cell viability was reported as a percentage of alive cells in treated and/or irradiated samples compared to control non-irradiated cells. Moreover, $1 \times 10^5$ or 200 AB22 cells from each differently treated flask were seeded in 10 cm diameter or in 6 cm diameter culture dishes for the proliferation assay or for the clonogenic assay, respectively.

For the proliferation assay, cell growth was monitored for 27 days from the neutron irradiation, and at predetermined time intervals, cells were washed with PBS, detached using 0.05% trypsin and 0.02% EDTA, and transferred in Falcon tubes. The cells were then sonicated for 30 s at 30% power in ice. The total cell protein concentration in the cell lysates, which is proportional to the number of cells, was determined using the Bradford method.

For the clonogenic assay, cells were allowed to grow for a duration of 16 days, with medium renewal every 2–3 days. After 16 days, the cells were washed with PBS, fixed in methanol for 25 min, and stained with a solution of 0.5% (w/v) Crystal Violet in 20% ethanol for 30 min. The excess of Crystal Violet was carefully removed, and the dishes were rinsed with tap water.

### 5.7. Animal model preparation

Adult male Balb/c mice were maintained in a specific pathogen-free environment at the animal facility of the Department of Molecular Biotechnology and Health Sciences at University of Turin, Italy. The care and handling of the animals followed the guidelines outlined in the EU Directive 2010/63/EU for animal experiments. The experimental

protocol involving animals was approved by the Italian Ministry of Health under Authorization Number 658/2021-PR.

AB22 cells were cultured as previously described, and tumours were induced by subcutaneously injecting $2.5 \times 10^6$ AB22 cells in a final volume of 0.15 mL GFNR Matrigel (CORNING Ref. 354,234): PBS (1:1 v/v) into the neck of each mouse. After ca. one week, the mice developed solid tumours with a volume of $60 \pm 20$ mm$^3$. At this time mice were ready for the treatment described in the following paragraph.

### 5.8. BNCT treatment on AB22 mesothelioma tumour bearing mice [64]

Using the same method described by Alberti et al. [63], F-CA-USF and NO$_2$-CA-USF treatments for mesothelioma-bearing mice was carried out, by using $^{10}$B enriched compounds, in the thermal column of the TRIGA Mark II reactor at Pavia University (Italy). The animal irradiation position was characterised in terms of neutron spectrum and background photon dose [71]. The irradiation facility designed for TAOrMINA treatment was originally intended to treat multiple liver metastases with BNCT. The animal irradiation chamber is 1 m long, 40 $\times$ 20 cm$^2$ in cross section, and begins around 1.3 m from the reactor core centre. To perform neutron irradiation, animals are positioned near the end of the chamber, with the reactor working at maximum power, where the in air thermal neutron flux is roughly $1.2 \times 10^{10}$ n/cm$^2$s. By doing this, the thermal neutron flow is maximised and the radiation duration is minimised (never exceeding 15 min).

20 tumour-bearing mice were divided into 6 groups: 1) control (CTRL, n = 4) non treated and not irradiated animals; 2) control irradiated with neutrons (CTRL IRR, n = 3); 3) treated with $^{10}$B-F-CA-USF ($^{10}$B-F-CA-USF, n = 3); 4) treated with $^{10}$B-NO$_2$-CA-USF ($^{10}$B-NO$_2$-CA-USF, n = 3); 5) treated with $^{10}$B-F-CA-USF and irradiated with neutrons ($^{10}$B-F-CA-USF IRR, n = 3); 6) treated with $^{10}$B-NO$_2$-CA-USF and irradiated with neutrons ($^{10}$B-NO$_2$-CA-USF IRR, n = 4). Irradiated and non-irradiated groups (3–6) have been treated, along 14 days, with 7 doses, (1 dose = 8.15 mg/kg of boron or 30 mg/kg of CA inhibitor) administered in the tail as an inclusion complex CA-inhibitor/cyclodextrin-polymer (MW = 125,000) (CA-inhibitor: poly- β-CD unit, molar ratio of 1:3.6). Briefly, 2 doses were injected at day 0, and the others at days 4,7,9,11,13. The first two doses were administered 22 h and the second 16 h before irradiation. The control groups (1 and 2) received at the same time the same volume of 0.9% saline solution. The concentration of DMSO was maintained always at 20%. The animals are exposed to the neutron field during the radiation treatment since the TRIGA Mark II's neutron field is not collimated. Neutron absorber shield composed of 95% $^6$Li-enriched Li$_2$CO$_3$ powder was utilised to minimise exposure of vital organs to neutrons. Due to the lack of secondary gamma radiation following thermal neutron capture, lithium-6 is the perfect isotope for creating efficient neutron shields for *in vivo* research. The Monte Carlo N-Particles (MCNP) simulation code was used to construct the treatment plan. By activating Cu wires using the Westcott formalism, neutron flux measurements were used to validate the simulation. Five mice were irradiated simultaneously according to the protocol used for the irradiation experiments. Each mouse was shielded from the radiation by two Li$_2$CO$_3$ neutron shield units, which covered the head and abdomen regions. To ensure that the tumours are exposed to the neutron flux directly, the units are kept about 1 cm apart.

### 5.9. Magnetic Resonance Imaging (MRI)

MR images of the mouse neck region were acquired on a 7 T Bruker Avance Neo AV300 spectrometer equipped with a Micro 2.5 micro-imaging probe and a birdcage resonator with 30-mm inner diameter. The tumour volume was measured from T$_2$-weighted MRI images obtained by using a rapid acquisition with refocused echoes sequence protocol (TR = 3500 ms; TE = 40.57 ms; number of slices = 20; slice thickness = 1 mm; FOV 40 $\times$ 40 mm; matrix 128 $\times$ 128). Animals were anesthetised before MRI examination by injecting tiletamine/zolazepam

(20 mg/kg; Zoletil 100, Virbac, Milan, Italy) and xylazine (5 mg/kg; Rompun, Bayer, Milan, Italy). The tumour volume was calculated using ITK-SNAP software by manually drawn a region of interest (ROI) covering the entire tumour region. The tumour volume enhancement (%) was determined using the following formula:

[(tumour volume (time = n) – tumour volume (time = 0)/tumour volume time = 0)] $\times$ 100, where time = 0 is referred to the volume of tumour before the first treatment, and time = n indicates the volume measured at various time intervals.

### 5.10. Inductively coupled plasma mass spectrometry (ICP-MS)

Boron content of CA inhibitor CA-SF, CA-USF, F-CA-USF and NO$_2$-CA-USF stock solution, and cell samples from uptake experiments were determined using inductively coupled plasma mass spectrometry (ICP-MS) (Element-2; Thermo-Finnigan, Rodano (MI), Italy). Sample digestion was performed using a high-performance Microwave Digestion System (ETHOS UP Milestone, Bergamo, Italy) after the addition of concentrated HNO$_3$ (70%) to CA inhibitor solutions or cell lysates (1:1), in a final volume of 0.4 mL. The amount of boron in cell samples measured by ICP-MS, was normalised to the protein content of each cell sample that was correlated to the number of cells by means of a calibration curve: [(mg protein)/(number of cells)]. The μg boron/g of tissue were thus calculated considering that 1 g of tissue contains $1 \times 10^8$ cells. The calibration curve was obtained using four boron absorption standard solutions (Sigma-Aldrich) in the range 0.1–0.004 μg/mL.

### CRediT authorship contribution statement

**Alberto Lanfranco:** Methodology, Investigation, Data curation. **Sahar Rakhshan:** Methodology, Investigation, Data curation. **Diego Alberti:** Writing – review & editing, Methodology, Data curation. **Polyssena Renzi:** Writing – review & editing, Methodology, Data curation. **Ayda Zarechian:** Investigation. **Nicoletta Protti:** Resources, Investigation, Funding acquisition, Data curation, Conceptualization. **Saverio Altieri:** Resources, Investigation, Data curation, Conceptualization. **Simonetta Geninatti Crich:** Writing – review & editing, Writing – original draft, Supervision, Resources, Funding acquisition, Data curation, Conceptualization. **Annamaria Deagostino:** Writing – review & editing, Writing – original draft, Resources, Funding acquisition, Data curation, Conceptualization.

### Declaration of competing interest

The authors declare that they have no known competing financial interests or personal relationships that could have appeared to influence the work reported in this paper.

### Data availability

Data will be made available on request.

### Appendix A. Supplementary data

Supplementary data to this article can be found online at https://doi.

org/10.1016/j.ejmech.2024.116334.

# References

[1] S.A. Saddoughi, Z.M. Abdelsattar, S.H. Blackmon, National trends in the epidemiology of malignant pleural mesothelioma: a national cancer data base study, Ann. Thorac. Surg. 105 (2018) 432–437.

[2] L. Berzenji, P. Van Schil, Multimodality treatment of malignant pleural mesothelioma, F1000Res (2018) 7.

[3] J. Cao, M.D. Zhang, B. Wang, L. Zhang, M.Y. Fang, F.F. Zhou, Chemoresistance and metastasis in breast cancer molecular mechanisms and novel clinical strategies, Front. Oncol. 11 (2021).

[4] S. Kannampuzha, A.V. Gopalakrishnan, Cancer chemoresistance and its mechanisms: associated molecular factors and its regulatory role, Med. Oncol. 40 (2023) 264.

[5] L. Gatti, F. Zunino, Overview of tumor cell chemoresistance mechanisms, Methods Mol. Med. (2005) 127–148.

[6] H.E. Barker, J.T. Paget, A.A. Khan, K.J. Harrington, The tumour microenvironment after radiotherapy: mechanisms of resistance and recurrence, Nat. Rev. Cancer 15 (2015) 409–425.

[7] X.F. Dai, Y.N. Luo, Y. Xu, J.Y. Zhang, Key indexes and the emerging tool for tumor microenvironment editing, Am. J. Cancer Res. 9 (2019) 1027–1042.

[8] J.A. Kemp, M.S. Shim, C.Y. Heo, Y.J. Kwon, "Combo" nanomedicine: Co-delivery of multi-modal therapeutics for efficient, targeted, and safe cancer therapy, Adv. Drug Deliv. Rev. 98 (2016) 3–18.

[9] S. Giovannuzzi, A. Nikitjuka, B.R. Pereira Resende, M. Smietana, A. Nocentini, C. T. Supuran, J.Y. Winum, Boron-containing carbonic anhydrases inhibitors, Bioorg. Chem. 143 (2024) 106976.

[10] C.T. Supuran, Carbonic Anhydrases as drug targets - an overview, Curr. Top. Med. Chem. 7 (2007) 825–833.

[11] C.T. Supuran, A. Scozzafava, Carbonic anhydrase inhibitors and their therapeutic potential, Expert Opin. Ther. Pat. 10 (2000) 575–600.

[12] C.T. Supuran, A. Scozzafava, Carbonic anhydrases as targets for medicinal chemistry, Bioorg. Med. Chem. 15 (2007) 4336–4350.

[13] J. Pastorek, S. Pastoreková, I. Callebaut, J.P. Mornon, V. Zelník, R. Opavský, M. Zat`ovicová, S. Liao, D. Portetelle, E.J. Stanbridge, et al., Cloning and characterization of MN, a human tumor-associated protein with a domain homologous to carbonic anhydrase and a putative helix-loop-helix DNA binding segment, Oncogene 9 (1994) 2877–2888.

[14] O. Türeci, U. Sahin, E. Vollmar, S. Siemer, E. Göttert, G. Seitz, A.K. Parkkila, G. N. Shah, J.H. Grubb, M. Pfreundschuh, W.S. Sly, Human carbonic anhydrase XII: cDNA cloning, expression, and chromosomal localization of a carbonic anhydrase gene that is overexpressed in some renal cell cancers, Proc. Natl. Acad. Sci. U.S.A. 95 (1998) 7608–7613.

[15] C.T. Supuran, Targeting carbonic anhydrases for the management of hypoxic metastatic tumors, Expert Opin. Ther. Pat. 33 (2023) 701–720.

[16] S. Singh, C.L. Lomelino, M.Y. Mboge, S.C. Frost, R. McKenna, Cancer drug development of carbonic anhydrase inhibitors beyond the active site, Molecules 23 (2018) 1045–1067.

[17] C. Lomelino, R. McKenna, Carbonic anhydrase inhibitors: a review on the progress of patent literature (2011-2016), Expert Opin. Ther. Pat. 26 (2016) 947–956.

[18] S.S. Shah, G. Rivera, M. Ashfaq, Recent advances in medicinal chemistry of sulfonamides. Rational design as anti-tumoral, anti-bacterial and anti-inflammatory agents, Mini Rev. Med. Chem. 13 (2013) 70–86.

[19] A. Scozzafava, C.T. Supuran, Carbonic anhydrase inhibitors. Arylsulfonylureido- and arylureido-substituted aromatic and heterocyclic sulfonamides: towards selective inhibitors of carbonic anhydrase isozyme I, J. Enzym. Inhib. 14 (1999) 343–363.

[20] F. Celik, M. Arslan, E. Yavuz, D. Demir, N. Gencer, Synthesis and carbonic anhydrase inhibitory properties of novel 1,4-dihydropyrimidinone substituted diarylureas, J. Enzym. Inhib. Med. Chem. 29 (2014) 18–22.

[21] K. Szafrański, J. Sławiński, Synthesis of novel 1-(4-substituted pyridine-3-sulfonyl)-3-phenylureas with potential anticancer activity, Molecules 20 (2015) 12029–12044.

[22] M. Bozdag, F. Carta, M. Ceruso, M. Ferraroni, P.C. McDonald, S. Dedhar, C. T. Supuran, Discovery of 4-Hydroxy-3-(3-(phenylureido)benzenesulfonamides as SLC-0111 analogues for the treatment of hypoxic tumors overexpressing carbonic anhydrase IX, J. Med. Chem. 61 (2018) 6328–6338.

[23] M. Bozdag, M. Ferraroni, C. Ward, F. Carta, S. Bua, A. Angeli, S.P. Langdon, I. H. Kunkler, A.M.S. Al-Tamimi, C.T. Supuran, Carbonic anhydrase inhibitors based on sorafenib scaffold: design, synthesis, crystallographic investigation and effects on primary breast cancer cells, Eur. J. Med. Chem. 182 (2019) 111600–111611.

[24] Y.-C. Wu, X.-Y. Ren, G.-W. Rao, Research progress of diphenyl urea derivatives as anticancer agents and synthetic methodologies, Mini-Reviews Org. Chem. 16 (2019) 617–630.

[25] K.J. Williams, R.G. Gieling, Preclinical evaluation of ureidosulfamate carbonic anhydrase IX/XII inhibitors in the treatment of cancers, Int. J. Mol. Sci. 20 (2019) 6080–6092.

[26] G. Vannozzi, D. Vullo, A. Angeli, M. Ferraroni, J. Combs, C. Lomelino, J. Andring, R. McKenna, G. Bartolucci, M. Pallecchi, L. Lucarini, S. Sgambellone, E. Masini, F. Carta, C.T. Supuran, One-pot procedure for the synthesis of asymmetric substituted ureido benzene sulfonamides as effective inhibitors of carbonic anhydrase enzymes, J. Med. Chem. 65 (2022) 824–837.

[27] M.A.A. Najm, W.R. Mahmoud, A.T. Taher, S.E.S. Abbas, F.M. Awadallah, H. A. Allam, D. Vullo, C.T. Supuran, Design and synthesis of some new benzoylthioureido phenyl derivatives targeting carbonic anhydrase enzymes, J. Enzym. Inhib. Med. Chem. 37 (2022) 2702–2709.

[28] F. Pacchiano, F. Carta, P.C. McDonald, Y. Lou, D. Vullo, A. Scozzafava, S. Dedhar, C.T. Supuran, Ureido-substituted benzenesulfonamides potently inhibit carbonic anhydrase IX and show antimetastatic activity in a model of breast cancer metastasis, J. Med. Chem. 54 (2011) 1896–1902.

[29] S. Kalinin, A. Malkova, T. Sharonova, V. Sharoyko, A. Bunev, C.T. Supuran, M. Krasavin, Inhibitors as candidates for combination therapy of solid tumors, Int. J. Mol. Sci. 22 (2021) 13405–13436.

[30] A.H. Soloway, W. Tjarks, B.A. Barnum, F.G. Rong, R.F. Barth, I.M. Codogni, J. G. Wilson, The chemistry of neutron capture therapy, Chem. Rev. 98 (1998) 1515–1562.

[31] M.F. Hawthorne, M.W. Lee, A critical assessment of boron target compounds for boron neutron capture therapy, J. Neuronc. 62 (2003) 33–45.

[32] M. Suzuki, Boron neutron capture therapy (BNCT): a unique role in radiotherapy with a view to entering the accelerator-based BNCT era, Int. J. Clin. Oncol. 25 (2020) 43–50.

[33] M.A. Dymova, S.Y. Taskaev, V.A. Richter, E.V. Kuligina, Boron neutron capture therapy: current status and future perspectives, Cancer Commun. 40 (2020) 406–421.

[34] M. Sasai, H. Nakamura, N. Sougawa, Y. Sakurai, M. Suzuki, C.M. Lee, Novel hyaluronan formulation enhances the efficacy of boron neutron capture therapy for murine mesothelioma, Anticancer Res. 36 (2016) 907–911.

[35] R.N. Grimes, Carboranes, 3nd Edition, third ed., Academic press, 2016.

[36] J.F. Valliant, K.J. Guenther, A.S. King, P. Morel, P. Schaffer, O.O. Sogbein, K. A. Stephenson, The medicinal chemistry of carboranes, Coord. Chem. Rev. 232 (2002) 173–230.

[37] A. Marfavi, P. Kavianpour, L.M. Rendina, Carboranes in drug discovery, chemical biology and molecular imaging, Nat. Rev. Chem 6 (2022) 486–504.

[38] F. Issa, M. Kassiou, L.M. Rendina, Boron in drug discovery: carboranes as unique pharmacophores in biologically active compounds, Chem. Rev. 111 (2011) 5701–5722.

[39] M. Scholz, E. Hey-Hawkins, Carbaboranes as pharmacophores: properties, synthesis, and application strategies, Chem. Rev. 111 (2011) 7035–7062.

[40] C. Alamón, B. Dávila, M.F. García, S. Nievas, M.A. Dagrosa, S. Thorp, M. Kovacs, E. Trias, R. Faccio, M. Gabay, N. Zeineh, A. Weizman, F. Teixidor, C. Viñas, M. Gavish, H. Cerecetto, M. Couto, A potential boron neutron capture therapy agent selectively suppresses high-grade glioma: *in vitro* and *in vivo* exploration, Mol. Pharm. 20 (2023) 2702–2713.

[41] V. Di Battista, E. Hey-Hawkins, Development of prodrugs for treatment of Parkinson's disease: new inorganic scaffolds for blood-brain barrier permeation, J. Pharmaceut. Sci. 111 (2022) 1262–1279.

[42] Y. Chen, F.K. Du, L.Y. Tang, J.R. Xu, Y.S. Zhao, X. Wu, M.X. Li, J. Shen, Q.L. Wen, C.H. Cho, Z.G. Xiao, Carboranes as unique pharmacophores in antitumor medicinal chemistry, Mol. Ther.-Oncol. 24 (2022) 400–416.

[43] Y.K. Au, Z.W. Xie, Recent advances in transition metal-catalyzed selective B-H functionalization of o-carboranes, Bull. Chem. Soc. Jpn. 94 (2021) 879–899.

[44] P. Stockmann, M. Gozzi, R. Kuhnert, M.B. Sarosi, E. Hey-Hawkins, New keys for old locks: carborane-containing drugs as platforms for mechanism-based therapies, Chem. Soc. Rev. 48 (2019) 3497–3512.

[45] Z.J. Lesnikowski, Recent developments with boron as a platform for novel drug design, Expert Opin. Ther. Pat. 11 (2016) 569–578.

[46] J. Nekvinda, M. Kugler, J. Holub, S. El Anwar, J. Brynda, K. Pospisilova, Z. Ruzickova, P. Rezacova, B. Gruener, Direct introduction of an alkylsulfonamido group on C-sites of isomeric dicarba-closo-dodecaboranes: the influence of stereochemistry on inhibitory activity against the cancer-associated carbonic anhydrase IX isoenzyme, Chem. Eur J. 26 (2020) 16541–16553.

[47] J. Brynda, P. Mader, V. Sicha, M. Fabry, K. Poncova, M. Bakardiev, B. Gruener, P. Cigler, P. Rezacova, Carborane-based carbonic anhydrase inhibitors, Angew. Chem., Int. Ed. 52 (2013) 13760–13763.

[48] J. Dvoranova, M. Kugler, J. Holub, V. Sicha, V. Das, J. Nekvinda, S. El Anwar, M. Havranek, K. Pospisilova, M. Fabry, V. Kral, M. Medvedikova, S. Matejkova, B. Liskova, S. Gurska, P. Dzubak, J. Brynda, M. Hajduch, P. Rezacova, Sulfonamido carboranes as highly selective inhibitors of cancer-specific carbonic anhydrase IX, Eur. J. Med. Chem. 200 (2020) 112460.

[49] M. Kugler, J. Nekvinda, J. Holub, S. El Anwar, V. Das, V. Sicha, K. Pospisilova, M. Fabry, V. Kral, J. Brynda, V. Kasicka, M. Hajduch, P. Rezacova, B. Gruener, Inhibitors of CA IX enzyme based on polyhedral boron compounds, Chembiochem 22 (2021) 2741–2761.

[50] B. Gruner, J. Brynda, V. Das, V. Sicha, J. Stepankova, J. Nekvinda, J. Holub, K. Pospisilova, M. Fabry, P. Pachl, V. Kral, M. Kugler, V. Masek, M. Medvedikova, S. Matejkova, A. Nova, B. Liskova, S. Gurska, P. Dzubak, M. Hajduch, P. Rezacova, Metallacarborane sulfamides: unconventional, specific, and highly selective inhibitors of carbonic anhydrase, J. Med. Chem. 62 (2019) 9560–9575.

[51] J. Fanfrlik, J. Brynda, M. Kugler, M. Lepsik, K. Pospisilova, J. Holub, D. Hnyk, J. Nekvinda, B. Gruner, P. Rezacova, B-H⋯π and C-H⋯π interactions in protein-ligand complexes: carbonic anhydrase II inhibition by carborane sulfonamides, Phys. Chem. Chem. Phys., 1728-1733.

[52] A. Pecina, M. Lepsik, J. Rezac, J. Brynda, P. Mader, P. Rezacova, P. Hobza, J. Fanfrlik, QM/MM calculations reveal the different nature of the interaction of two carborane-based sulfamide inhibitors of human carbonic anhydrase II, J. Phys. Chem. B 117 (2013) 16096–16104.

[53] P. Mader, A. Pecina, P. Cigler, M. Lepsik, V. Sicha, P. Hobza, B. Gruner, J. Fanfrlik, J. Brynda, P. Rezacova, Carborane-based carbonic anhydrase inhibitors: insight into CAII/CAIX specificity from a high-resolution crystal structure, modeling, and quantum chemical calculations, BioMed Res. Int. (2014) 389869–389878.

[54] M. Kugler, J. Holub, J. Brynda, K. Pospisilova, S.E. Anwar, D. Bavol, M. Havranek, V. Kral, M. Fabry, B. Gruner, P. Rezacova, The structural basis for the selectivity of sulfonamido dicarbaboranes toward cancer-associated carbonic anhydrase IX, J. Enzym. Inhib. Med. Chem. 35 (2020) 1800–1810.

[55] J. Sforzi, A. Lanfranco, R. Stefania, D. Alberti, V. Bitonto, S. Parisotto, P. Renzi, N. Protti, S. Altieri, A. Deagostino, S. Geninatti Crich, A novel pH sensitive theranostic PLGA nanoparticle for boron neutron capture therapy in mesothelioma treatment, Sci. Rep. 13 (2023) 620.

[56] A. Lanfranco, D. Alberti, S. Parisotto, P. Renzi, V. Lecomte, S. Geninatti Crich, A. Deagostino, Biotinylation of a MRI/Gd BNCT theranostic agent to access a novel tumour-targeted delivery system, Org. Biomol. Chem. 20 (2022) 5342–5354.

[57] D. Alberti, A. Michelotti, A. Lanfranco, N. Protti, S. Altieri, A. Deagostino, S. Geninatti Crich, *In vitro* and *in vivo* BNCT investigations using a carborane containing sulfonamide targeting CAIX epitopes on malignant pleural mesothelioma and breast cancer cells, Sci. Rep. 10 (2020) 19274.

[58] A. Innocenti, A. Scozzafava, S. Parkkila, L. Puccetti, G. De Simone, C.T. Supuran, Investigations of the esterase, phosphatase, and sulfatase activities of the cytosolic mammalian carbonic anhydrase isoforms I, II, and XIII with 4-nitrophenyl esters as substrates, Bioorg. Med. Chem. Lett. 18 (2008) 2267–2271.

[59] S.M. Gould, D.S. Tawfik, Directed evolution of the promiscuous esterase activity of carbonic anhydrase II, Biochemistry 44 (2005) 5444–5452.

[60] M.F. Ansari, D. Idrees, M.I. Hassan, K. Ahmad, F. Avecilla, A. Azam, Design, synthesis and biological evaluation of novel pyridine-thiazolidinone derivatives as anticancer agents: targeting human carbonic anhydrase IX, Eur. J. Med. Chem. 144 (2018) 544–556.

[61] N.R. Uda, V. Seibert, F. Stenner-Liewen, P. Müller, P. Herzig, G. Gondi, R. Zeidler, M. van Dijk, A. Zippelius, C. Renner, Esterase activity of carbonic anhydrases serves as surrogate for selecting antibodies blocking hydratase activity, J. Enzym. Inhib. Med. Chem. 30 (2015) 955–960.

[62] M. Khan, S.K. Avula, S.A. Halim, M. Waqas, M. Asmari, A. Khan, A. Al-Harrasi, Biochemical and in silico inhibition of bovine and human carbonic anhydrase-II by 1H-1,2,3-triazole analogs, Front. Chem. 10 (2022) 1072337.

[63] E. Azzi, D. Alberti, S. Parisotto, A. Oppedisano, N. Protti, S. Altieri, S. Geninatti-Crich, A. Deagostino, Design, synthesis and preliminary in-vitro studies of novel boronated monocarbonyl analogues of Curcumin (BMAC) for antitumor and β-amiloyd disaggregation activity, Bioorg. Chem. 93 (2019) 103324–103334.

[64] U. Del Monte, Does the cell number 109 still really fit one gram of tumor tissue? Cell Cycle 8 (2009) 505–506.

[65] H. Kim, J. Han, J.H. Park, Cyclodextrin polymer improves atherosclerosis therapy and reduces ototoxicity, J. Contr. Release 319 (2020) 77–86.

[66] X. Li, H. Liu, J. Li, Z. Deng, L. Li, J. Liu, J. Yuan, P. Gao, Y. Yang, S. Zhong, Micelles via self-assembly of amphiphilic beta-cyclodextrin block copolymers as drug carrier for cancer therapy, Colloids Surf. B Biointerfaces 183 (2019) 110425.

[67] J. Cheng, K.T. Khin, M.E. Davis, Antitumor activity of β-cyclodextrin Polymer−Camptothecin conjugates, Mol. Pharm. 1 (2004) 183–193.

[68] D.A. Gruzdev, A.V. Vakhrushev, A.M. Demin, M.A. Baryshnikova, G.L. Levit, V. P. Krasnov, V.N. Charushin, Synthesis of closo- and nido-carborane derivatives of the KRGD peptide, J. Organomet. Chem. 1008 (2024) 123052.

[69] F. Campo, M. Mossotti, L. Panza, Synthesis of complex glycosylated carboranes for BNCT, Synlett 2012 (2012) 120–122.

[70] J.G. Wilson, A.K.M. Anisuzzaman, F. Alam, A.H. Soloway, Development of carborane synthons: synthesis and chemistry of (aminoalkyl)carboranes, Inorg. Chem. 31 (1992) 1955–1958.

[71] S. Bortolussi, N. Protti, M. Ferrari, I. Postuma, S. Fatemi, M. Prata, F. Ballarini, M. P. Carante, R. Farias, S.J. González, M. Marrale, S. Gallo, A. Bartolotta, G. Iacoviello, D. Nigg, S. Altieri, Neutron flux and gamma dose measurement in the BNCT irradiation facility at the TRIGA reactor of the University of Pavia, Nucl. Instruments Methods Phys. Res. Sect. B Beam Interact. Mater. Atoms 414 (2018) 113–120.